From the DEPARTMENT OF NEUROSCIENCE
Karolinska Institutet, Stockholm, Sweden

NOVEL TOOLS FOR THE STUDY AND DIAGNOSIS OF BACTERIAL INFECTIONS

Exploring the intersection of microbiology and microfabrication

Haris Charalampos Antypas

Karolinska Institutet

Stockholm 2018

Cover design by Iraklis Papaeracleous
All previously published papers were reproduced with permission from the publisher
Published by Karolinska Institutet
Printed by E-Print AB 2018

ISBN 978-91-7831-172-9

NOVEL TOOLS FOR THE STUDY AND DIAGNOSIS OF BACTERIAL INFECTIONS

Exploring the intersection of microbiology and microfabrication

THESIS FOR DOCTORAL DEGREE (Ph.D.)

ACADEMIC DISSERTATION

Public defence in Biomedicum 1 lecture hall
Solnavägen 9, Karolinska Institutet
Stockholm, Sweden

Friday October 12th, 2018, 13:00

By

Haris Charalampos Antypas

Principal Supervisor:
Professor Agneta Richter-Dahlfors
Karolinska Institutet
Swedish Medical Nanoscience Center
Department of Neuroscience

Co-supervisor:
Professor Mikael Rhen
Karolinska Institutet
Department of Microbiology, Tumor and Cell Biology

Opponent:
Senior lecturer Linus Sandegren
Uppsala University
Department of Medical Biochemistry and Microbiology

Examination Board:
Assistant Professor Anna Herland
KTH Royal Institute of Technology
Department of Micro and Nanosystems

Professor Roland Möllby
Karolinska Institutet
Department of Microbiology, Tumor and Cell Biology

Professor Bernt Eric Uhlin
Umeå University
Department of Molecular Biology

To my parents,

Konstantinos and Paraskevi,

without whom none of my success would be possible

ABSTRACT

The alarming increase in antibiotic resistance calls for new approaches to study and diagnose bacterial infections. In my thesis, I worked at the intersection of microbiology, microfabrication, and optical probes to develop novel diagnostic and screening assays for microbiology and elucidate bacterial pathogenesis in urinary tract infections (UTI).

Conventional antibiotic susceptibility testing (AST) has an 18 h turnaround time and low throughput. P**apers I & II** describe the development and validation of the nanowell AST (nwAST). This method was based on the nanowell slide (nwSlide), which is a miniaturized nanotiter well plate featuring 672 nanowells of 500 nl each. Owing to this large number of wells, we designed a quantitative AST that determines a minimum inhibitory concentration for up to 6 antibiotics. Validation with 70 UPEC clinical isolates showed a 97.9 % overall categorical agreement with agar disc diffusion and a turnaround time between 3 h 40 min - 8 h 10 min. Key to this short turnaround time was the implementation of the T_{lag} algorithm, which identified the exact time point when bacteria started to grow. This analysis delivered results up to 5 times faster compared to conventional AST. Overall, our high throughput nwAST surpassed FDA's requirement of > 90 % categorical agreement.

The agar plate and 96-well plate offer a limited resolution for bacterial phenotypic screening. To improve screening resolution, in **paper III** we took advantage of the nwSlide's versatility and combined it with fluorescence-activated cell sorting. We developed a rapid workflow to directly select and single-sort bacterial mutants in individual nanowells, based on a fluorescence-encoding transposon. Sorted mutants were phenotypically screened for growth, morphology, and metabolism already during the first incubation on the nanowell slide using spectrophotometry, algorithmic analysis and microscopy. Selected phenotypes were retrieved and screened with single-primer PCR and sequencing to identify the transposon insertion site. By leveraging the versatility of the nwSlide, we developed a high-resolution screening platform, with higher throughput and less reagent consumption compared to the agar plate and 96-well plate.

In **paper IV,** we developed a proximal tubule-on-a-chip (PToC) based on a microfluidic device. We delineated UPEC's adhesion to renal epithelial cells under shear stress with temporal and single-cell resolution. We demonstrated that only a minority of cells adhered and withstood shear stress for > 30 min. This binding was PapG-independent. Adherent bacteria divided rapidly and eventually formed microcolonies, which were mediated by FimH adhesin. Microcolonies expanded colonization beyond the cell surface, enhanced infection spread, and extended bacterial binding under shear stress from minutes to hours. Although the absence of PapG and FimH delayed infection, UPEC eventually colonized renal cells causing them to round up and slough off. These results showed that UPEC has a repertoire of redundant adhesion organelles that help bacteria to withstand shear stress in the urinary tract.

Detection of biofilm is absent in clinical diagnostics, despite its association with antibiotic tolerance. In **paper V,** we developed a rapid diagnostic assay for biofilm-associated UTI

called optotracing. This assay is based on heptamer formyl thiophene acetic acid, a luminescent conjugated oligothiophene. This molecule produces a unique spectral signature upon binding to cellulose, which is an extracellular component in biofilms of UPEC. We first optimized optotracing's performance in PBS and healthy urine spiked with UPEC biofilm or purified cellulose. Next, we developed a workflow to isolate and screen urine sediment for cellulose within 45 min. Optotracing of 182 urine samples from UTI patients and interpretation of results with principal component analysis and k-means clustering identified 27 urine samples as positive for cellulose. This result provided the first direct evidence of biofilm formation in UTI. With a short turnaround time and minimum equipment requirement, this diagnostic assay could guide clinicians when choosing antibiotics for biofilm-associated infections.

POPULAR SCIENCE SUMMARY

The widespread emergence of antibiotic resistance has brought bacterial infections back to the spotlight. Today, more than ever, there is a need to increase our understanding of bacterial pathogenesis and apply this knowledge on new approaches for prevention, diagnosis, and treatment. In my thesis, I combined microbiology with new technologies to improve the study and diagnosis of urinary tract infections.

Clinicians often have no choice but to prescribe antibiotics based on a clinical educated guess, as diagnostics to identify the right treatment may take several days to deliver results. However, this approach can be ineffective and it can also promote harmless bacteria in our body to become resistant. In **papers I & II,** we developed a diagnostic test to help clinicians choose the right antibiotic. This test was based on the nanowell slide, a miniature device that fits in the palm of a hand. In the 672 tiny wells of the nanowell slide, bacteria were incubated with different antibiotics. Based on the amount of light that passed through the transparent bottom of these wells, we could understand how bacteria responded to antibiotics. A decreasing amount of light indicated growth of resistant bacteria, whereas a constant high amount of light indicated inhibition of susceptible bacteria. Key to rapid diagnosis was an algorithm that processed the changes of light and detected resistant bacteria within 3-8 h. The accurate and timely diagnosis of this test could help clinicians prescribe the right antibiotic fast, thus improving patient outcome and reducing antibiotic resistance.

The ability of bacteria to thrive in so many different environments lies in their genes. However, it is not always easy to pinpoint the genes behind different characteristics of bacteria. In **paper III,** we approached this problem by randomly "turning off" bacterial genes. Hundreds of bacteria with different genes deactivated were encapsulated one by one in small droplets and added in the nanowell slide. While they multiplied in the wells, we examined them in detail with light measurements, microscopy, and algorithmic analysis. Bacteria with abnormal growth, metabolism, and morphology were picked to identify which of their genes had been deactivated. By doing so, we associated specific genes with different bacterial characteristics. Using our approach, microbiologists could understand the role of bacterial genes in a more detailed and user-friendlier way compared to other methods.

Uropathogenic bacteria can move up in the urinary tract and infect the kidneys without being flushed away by urine. In **paper IV,** we simulated the kidney environment in a device with small transparent channels to understand how bacteria resist urine flow. Each channel contained a single layer of kidney cells, which was exposed to uropathogenic *Escherichia coli* under flow conditions. Using time-lapse microscopy, we saw that only a few bacteria were fit enough to attach to cells. These so-called "settlers" of the infection multiplied rapidly, forming small colonies on the cells. Colonies protected bacteria against the flow and produced new bacteria to spread the infection. Key to the resistance of settlers and colonies against the flow was some sticky rods on bacteria's surface. Using these rods called fimbriae, bacteria attached to renal cells, but also to each other to form microcolonies. Understanding how bacteria cause infection can lead to better prevention and treatment. Moreover,

replication of organ functions in devices has the potential to reduce and replace the use of experimental animals.

Bacteria living in colonies covered with a slimy film of proteins and polysaccharides are known as biofilms. In a biofilm, bacteria are more tolerant to antibiotics than they are alone. Therefore, if a biofilm forms in a patient, it can lead to a chronic infection. Despite posing a threat to our health, there are currently no diagnostic methods for biofilm. In **paper V,** we used a fluorescent molecule to develop the first diagnostic test for biofilm in urinary tract infections. This molecule detects cellulose, a biofilm component of uropathogenic *Escherichia coli*. Based on this property, we screened 182 urine samples from UTI patients and identified 27 as cellulose-positive. Because humans do not produce cellulose, its detection in urine showed that bacteria had formed biofilm in the urinary tract of these patients. The possibility to detect biofilm could help clinicians prescribe better-tailored antibiotic therapies to patients.

LIST OF SCIENTIFIC PAPERS

I. Weibull E, **Antypas H**, Kjäll P, Brauner A, Andersson-Svahn H, Richter-Dahlfors A. Bacterial nanoscale cultures for phenotypic multiplexed antibiotic susceptibility testing. *Journal of Clinical Microbiology*. 2014;52(9):3310-3317.

II. Veses-Garcia M, **Antypas H**, Löffler S, Brauner A, Andersson-Svahn H, Richter-Dahlfors A. Rapid phenotypic antibiotic susceptibility testing of uropathogens using optical signal analysis on the nanowell slide. *Frontiers in Microbiology*. 2018;9:1530.

III. **Antypas H**, Veses-Garcia M, Weibull E, Andersson-Svahn H, Richter-Dahlfors A. A universal platform for selection and high-resolution phenotypic screening of bacterial mutants using the nanowell slide. *Lab on a Chip*. 2018;18(12):1767-1777.

IV. **Antypas H** & Richter-Dahlfors A. Single-cell studies of uropathogenic *Escherichia coli* fitness determinants during colonization of epithelial cells under shear stress. *Manuscript.*

V. **Antypas H**, Choong FX, Libberton B, Brauner A, Richter-Dahlfors A. Rapid diagnostic assay for detection of cellulose in urine as biomarker for biofilm-related urinary tract infections. *Manuscript submitted for publication.*

Published work conducted during my doctoral studies but not included in the thesis:

- Choong FX, **Antypas H**, Richter-Dahlfors A. Integrated pathophysiology of pyelonephritis. *Microbiology Spectrum*. 2015;3(5)

- **Antypas H**, Libberton B, Melican K. Reducing background cytokine expression in epithelial cells without serum starvation. *MethodsX*. 2014;1:251-253.

Patent applications produced during my doctoral studies:

- Richter-Dahlfors A, Libberton AB, Nilsson P, Bäck M, Löffler S, Shirani Bidabadi H, Choong X, **Antypas C**. Detection of microbial peptides. WO/2017/058085.

CONTENTS

LIST OF ABBREVIATIONS

AST	Antibiotic Susceptibility Testing
E. coli	*Escherichia coli*
ECM	Extracellular Matrix
FACS	Fluorescence-Activated Cell Sorting
FISH	Fluorescence *In Situ* Hybridization
GFP	Green Fluorescent Protein
h-FTAA	Heptamer Formyl Thiophene Acetic Acid
LCO	Luminescent Conjugated Oligothiophene
MIC	Minimum Inhibitory Concentration
MUG	4-Methylumbelliferyl β-D-Galactopyranoside
nOSAT	nanoculture Optical Signal Analysis Tool
nwAST	nanowell Antibiotic Susceptibility Testing
nwSlide	nanowell Slide
PToC	Proximal Tubule-on-a-Chip
SCTA	Single-Cell Trajectory Analysis
UPEC	Uropathogenic *Escherichia coli*
UTI	Urinary Tract Infection
WT	Wild Type

1 INTRODUCTION

1.1 THE RISE OF ANTIBIOTIC RESISTANCE

The monumental discovery of penicillin by Sir Alexander Fleming in 1929 *(1)*, followed by a golden age of antibiotic discovery between 1950-1960, made antibiotics the bedrock of modern medicine and heralded the end of bacterial infections as a health threat *(2)*. Fast forward to 2018, and health organizations are devising action plans to face a post-antibiotic era *(3–5)*. Antibiotic resistant "superbugs" make headlines every week, and the pipeline for new antibiotics is drying out *(6)*. It is estimated that 25,000 people in Europe and 23,000 people in the United States die every year due to infections from antibiotic resistant bacteria *(3, 4)*. What led to the emergence of antibiotic resistance should come as no surprise. During his Nobel Lecture on penicillin in 1945, Fleming had already warned:

> The time may come when penicillin can be bought by anyone in the shops. Then there is the danger that the ignorant man may easily underdose himself and by exposing his microbes to non-lethal quantities of the drug make them resistant. *(7)*

Indeed, misuse, but also indiscriminate overuse of antibiotics, has led to a high selective pressure among bacteria, and unavoidably to development of resistance *(8)*. However, the early euphoria surrounding antibiotics and the high discovery rate of new antibiotics in previous decades made us underestimate the ability of bacteria to evolve in the long run. The exclusive reliance on antibiotic treatment came at the expense of infection research, prevention, and diagnosis. Today, besides antibiotic discovery, bacterial pathogenesis itself has to be revisited. Since the dawn of modern microbiology in Koch's era, causality between pathogen and disease has proved complex. Multifactorial virulence, heterogeneity, and biofilms are some of the concepts that require thorough investigation to unravel the complexity of bacterial pathogenesis fully. Findings deriving from the study of bacterial pathogenesis should serve as the cornerstone for improving prevention, diagnosis, and treatment to deal with antibiotic resistance. In these efforts, technology should play a central role to move the field of microbiology forward.

1.2 CAUSALITY BETWEEN BACTERIA AND DISEASE

Despite bacteria's 3-billion-year presence on our planet, it was not until the 17th century when Antonie van Leeuwenhoek directly observed them with his microscopes *(9)*. It took 2 more centuries before causality between bacteria and disease was established by Robert Koch *(10)*. His pioneering work in microscopy techniques, *in vitro* bacterial cultures, and animal models enabled Koch to demonstrate bacteria as causative agents for anthrax, cholera, and tuberculosis *(10)*. While researching the etiology of tuberculosis, he proposed 4 postulates as a framework to establish causality between bacteria and disease *(11)*:

(i) Bacteria should be present only in diseased and not in healthy individuals
(ii) Bacteria should be isolated in pure culture
(iii) Isolated bacteria should cause the disease in a healthy experimental host

(iv) Bacteria should be isolated anew from the diseased experimental host

Although these postulates led to the identification of several new pathogens, they were not universal *(12)*. As new molecular methods became available, microbiologists obtained a more refined view of bacterial pathogenesis. Not only was disease linked to specific bacteria, but also to specific genes, termed virulence factors. Based on this new knowledge, the Koch's postulates were modified into the Molecular Koch's postulates *(12, 13)*:

(i) The gene suspected to cause disease should be present only in virulent and not in avirulent bacteria
(ii) Inactivation of the gene should mitigate pathogenicity or introduction of the gene in an avirulent strain should confer pathogenicity
(iii) The gene should be expressed in the host during infection

The original and molecular postulates have a conceptual and technical aspect *(14)*. The conceptual aspect concerns the natural disease development and microbial pathogenesis, whereas the technical aspect encompasses the methods available to detect, isolate and culture bacteria or to manipulate their genome. Looking at causality through the conceptual aspect, we can identify several examples from infection biology that fail to conform to the postulates. Pathogenicity is not only an intrinsic bacterial property, but it also depends on the microbe-host interaction. For instance, bacteria avirulent by definition can turn into opportunistic pathogens when the host's immune system becomes compromised *(15)*, or benign commensal bacteria of the intestinal flora can cause disease upon entry to a different body site (Fig. 1) *(12)*. Multifactorial virulence is another example where conceptual and technical aspects of the postulates are not satisfied. The ability of bacteria to cause disease can be traced not only back to one, but also back to a synergy of virulence factors (Fig. 1). Inactivation of single virulence factors in acute infections, such as the toxin of *Vibrio cholerae* or the capsule of *Streptococcus pneumoniae*, led to an apparent loss of pathogenicity *(13, 16)*. In other infections, however, virulence factors deviate from their traditional definition. Their role is contributory instead of requisite, and they act in synergy with other factors *(16)*. As they confer a competitive advantage without being a prerequisite for infection establishment, they are better described as fitness factors *(17, 18)*. These factors can be transiently and heterogeneously expressed in a bacterial population, depending on the infection stage and the cues from the host's microenvironment *(12)(19)*. Biofilm-associated infections are yet another group of infections that departs from the conceptual aspects of the postulates (Fig. 1). Biofilms can be mono- or polymicrobial, with a different microbial composition among patients suffering from the same type of infection *(20)*. Their formation is orchestrated by complex gene networks in response to several external cues, making it difficult to link the disease to specific bacterial factors.

Addressing these new concepts of bacterial pathogenesis can be technically hard. To investigate the role of the immune system and host tissue in bacterial pathogenesis, clinically and physiologically relevant infection models are needed. Assessing the role of fitness factors

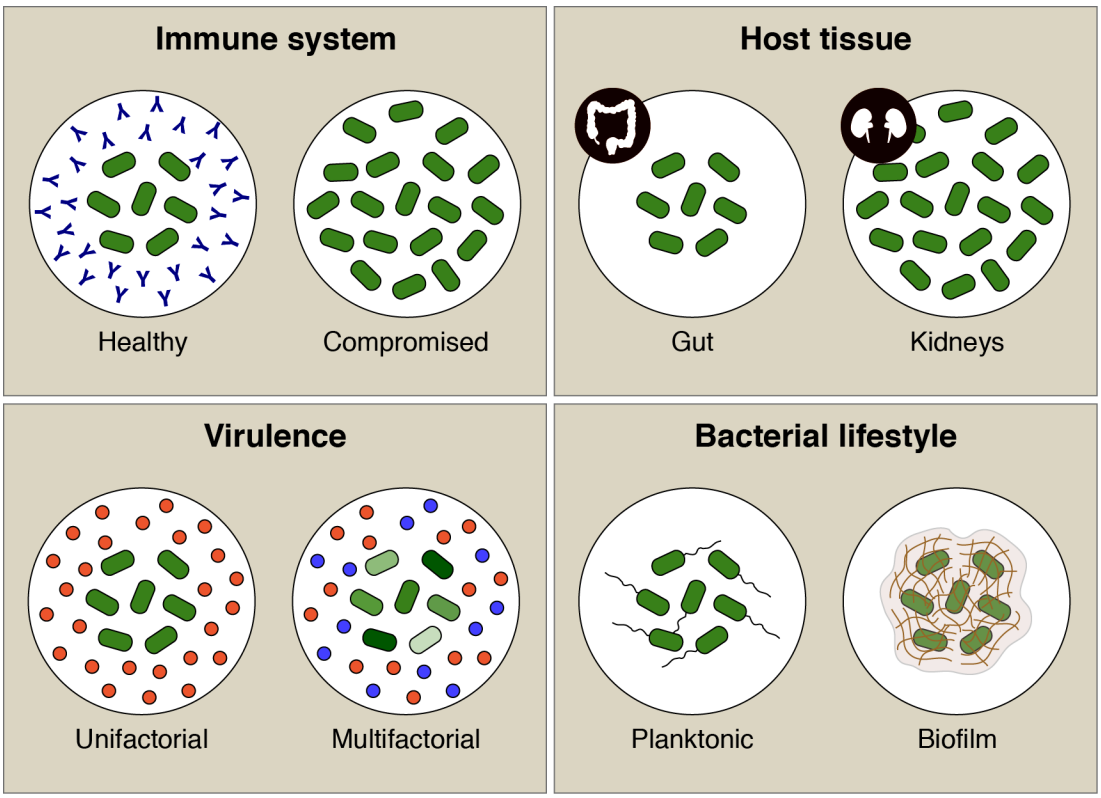

Fig. 1 Examples of bacterial pathogenesis outside the conceptual scope of the original and molecular Koch's postulates. Bacterial pathogenicity can depend on the status of the host immune system (top left panel) and the anatomical site of the host (top right panel). It can be mediated by a single virulence factor, which is a prerequisite for the infection, or by several factors with a contributory role to overall virulence (bottom left panel). Expression of these factors can be heterogeneous in the bacterial population (bottom left panel). Bacterial pathogenicity can also depend on the bacterial lifestyle, with planktonic bacteria associated with acute infections and biofilm with chronic infections (bottom right panel).

requires models with spatiotemporal resolution. This resolution is currently lacking in sacrificial animal models, where infection is examined at the infection endpoint by measuring the bacterial load in harvested organs or by performing an immunohistological examination *(13)*. Phenotypic bacterial heterogeneity requires yet another parameter to be added in infection models: the single-cell resolution. Finally, detection of biofilm-associated infections is currently absent. New biofilm-specific methods need to be developed, as current diagnostics are designed to detect, isolate and grow planktonic bacteria.

Through these examples, it becomes evident that Koch's original and molecular postulates are not to be used as dogma, but rather as a guide to scientific thinking. However, even when an infection does not fulfill a postulate, it should be seen as an opportunity to understand bacterial pathogenesis better. In the following sections, we describe how technical innovations can help us understand the role of tissue physiology, multifactorial virulence, and biofilm in urinary tract infections, which are cases of bacterial pathogenesis that fall outside the conceptual scope of the postulates.

1.2.1 Spatiotemporal studies of bacterial pathogenesis in pyelonephritis: The paradigm of P and Type 1 fimbriae synergy

Pyelonephritis represents an upper urinary tract infection (UTI) targeting the kidneys. More than 70 % of acute cases of pyelonephritis are caused by Uropathogenic *Escherichia coli* (UPEC) *(21)*, an otherwise benign commensal in the gut flora *(22)*. Typically, bacteria enter the urinary tract through the urethra and eventually reach the bladder, where they cause cystitis *(23)*. Further ascension to the kidneys via the ureters leads to pyelonephritis, which is characterized as a tubulointerstitial disorder *(24)*. Although less common than cystitis, pyelonephritis entails the risk of leading to urosepsis *(25)*.

The kidney, a normally sterile organ, is anatomically and physiologically challenging for bacteria to infect *(26)*. The morphology of the renal epithelium is far from uniform along its different segments *(27)* and constantly descending flow of urine generates shear stress along this single-layer epithelium. Infection establishment under these conditions depends on UPEC's ability to bind specific host cell receptors on the renal epithelium and to withstand shear stress. Binding is conferred by a group of adhesion organelles, called fimbriae *(28)*. A fimbrial operon encountered in ≈ 80 % of pyelonephritic isolates is the *pap* operon, which encodes P fimbriae *(29)*. This high prevalence of *pap* operon suggested that P fimbriae provide UPEC with an advantage to infect the kidneys. Indeed, P fimbriae bind via their PapG tip adhesin to Gal(α1-4)Gal moieties found on the glycolipid globoseries of the renal epithelium *(30–33)*. PapG has three variants, classes I, II and III, with class II mainly associated with pyelonephritis in humans *(34, 35)*. Although several studies have been performed using sacrificial animal models of the ascending UTI, findings on the role of P fimbriae in pyelonephritis are inconsistent *(36)*. Differences in animal models, UPEC strains and mutagenesis methods used may account for these inconsistencies *(36)*. For instance, a study conducted with a P fimbrial mutant of UPEC strain HU734 showed reduced bacterial loads in kidneys of CBA mice *(37)*, whereas another study in the same mouse model using an isogenic *papG* mutant of UPEC CFT073 showed only a subtle role for P fimbriae *(38)*. Mutants were constructed with chemical mutagenesis in the first study and allelic exchange mutagenesis in the second. Therefore, secondary mutations caused by the less precise chemical mutagenesis may have accounted for the decreased virulence observed. In a third study using the isogenic *papG* mutant of UPEC DS17 in a monkey model, renal pathology was attenuated compared to WT infection *(39)*. PapG receptors are present in both mice and monkeys, but differences in the patterns of isoreceptors may affect host specificity *(40)*. Additionally, we have to take into account that the immune response to P fimbriae differs among animal models *(36)*. Regardless of the results, all these studies performed in sacrificial animal models had one thing in common. They were investigating the role of P fimbriae solely in the context of the infection outcome. Real-time monitoring of pyelonephritis, using the 2-photon microscopy-based intravital rat model, provided new insight into the role of P fimbriae *(41)*. In this model UPEC CFT073 rapidly colonized the renal proximal tubule, leading to major alterations in tissue homeostasis. When compared to an isogenic *papG* mutant, it was shown that P fimbriae enhanced initial adhesion to the

epithelium of proximal tubules, but they were not a requirement for the establishment of pyelonephritis, suggesting that P fimbriae act as a fitness rather than a virulence factor *(42)*.

By studying pyelonephritis in the intravital rat model under a spatiotemporal resolution, a new role was also shown for Type 1 fimbriae. These fimbriae, which are encoded by operon *fim*, are present in virtually all UPEC strains *(43, 44)*. They are traditionally associated with cystitis, where they mediate adhesion to the bladder epithelium *(45, 46)*. Their tip adhesin, FimH, binds to the terminally exposed mannose residues of Uroplakin Ia. This is a major protein of the urothelial plaques found on the superficial umbrella cells comprising the bladder epithelium *(45–47)*. Besides this role, the intravital model showed that FimH enabled bacteria to expand colonization towards the lumen of the proximal tubule, leading to nephron obstruction *(42)*. This finding suggested that FimH mediates interbacterial interactions by binding to mannose residues of LPS *(48)*. Similar to PapG, FimH was not a prerequisite for infection establishment *(42)*. Therefore, both adhesins act rather as fitness factors. Through their synergistic action, UPEC better withstands the flow of primary filtrate in the proximal tubules, resulting in a faster and more efficient progression of the infection. This highlights the need to use spatiotemporal rather than sacrificial animal models to obtain the full picture of bacterial pathogenesis.

1.2.2 Bacterial biofilms in infection: An emerging threat

Biofilm has emerged during the last 3 decades from an overlooked parameter of bacterial infections to an important contributor of pathogenicity. The term biofilm describes a sessile bacterial lifestyle in which bacteria form multicellular aggregated communities embedded in a self-secreted extracellular matrix (ECM), composed of proteins, polysaccharides, lipids and extracellular DNA *(49)*. The ECM defines a biofilm spatially, affecting parameters such as interbacterial interactions, communication with the external environment and nutrient distribution *(50)*. As a result, bacteria in biofilms exhibit different properties compared to bacteria in a planktonic lifestyle. Whereas planktonic bacteria usually cause acute infections, biofilms are often associated with chronic infections, characterized by tolerance to the host's immune response and clinically relevant doses of antibiotics *(51)*. Tolerance to antibiotics derives from the distinct physiology of bacteria in biofilms, the complex biofilm structure itself, but also from the specific microenvironmental conditions at the infection site *(52–59)*. Despite the far more severe consequences of biofilm-associated infections, it remains a challenge to differentiate between biofilm and planktonic bacteria in a patient.

1.2.2.1 Diagnostic challenges in biofilm-associated infections

Diagnostic methods routinely used for bacterial infections were developed with the planktonic lifestyle in mind, and they are inadequate to detect biofilm in a patient. Biofilm in infection results from phenotypic changes triggered by the host’s environment. Consequently, this phenotype is quickly lost in culture-based methods, in which bacteria are subcultured from a patient sample under conditions that promote planktonic growth *(60)*. Molecular methods, such as PCR-based detection of bacterial genes, cannot distinguish either between

the distinct phenotype of biofilm and planktonic bacteria, as they detect genotypic traits *(61–63)*. Therefore, biofilm diagnostics should take place directly in a patient sample and detect biofilm-specific phenotypic traits. What clearly distinguishes a biofilm from planktonic bacteria is the presence of bacterial aggregates encased in an ECM. Bacterial aggregates can be detected directly in a patient sample with light microscopy using non-specific staining (e.g., Gram stain) or with confocal microscopy using species-specific fluorescent probes (e.g., fluorescence *in situ* hybridization (FISH) and peptide nucleic acid FISH) *(64, 65)*. Detection of ECM components, however, is lagging behind. Carbohydrates in the ECM have been visualized using several non-specific stains, such as alcian blue, calcofluor, ruthenium red *(66, 67)* and fluorescently labeled lectins *(68, 69)*, but the interpretation of results is somewhat subjective. Immunostaining of biofilm-specific antigens has been applied only in a few cases. Such examples are the detection of alginate in *Pseudomonas aeruginosa* biofilms with immunofluorescence *(64)*, and detection of curli in UPEC with electron microscopy *(70)*. However, sample preparation in these approaches is laborious and time-consuming. Moreover, confocal and electron microscopy are not suitable for routine use in a clinical lab, where hundreds of samples arrive daily.

1.2.2.2 Luminescent conjugated oligothiophenes as a new tool for biofilm detection

A group of fluorophore reporters, called luminescent conjugated oligothiophenes (LCO), holds promise as a new approach for the diagnosis of biofilm-related infections. LCO consist of a defined oligothiophene backbone, which forms an extended conjugated π-system *(71–73)*. Binding of LCO to a target molecule via non-covalent electrostatic and hydrophobic interactions causes the oligothiophene backbone to assume a distinct conformation, which distorts the extension of the conjugated π-system. This distortion changes the energy gap between the ground and the first excited singlet state, which generates a target-specific optical signature *(73)*. Based on this property, LCO act as conformation sensitive optical probes. Heptamer formyl thiophene acetic acid (h-FTAA), a molecule of the LCO group, generates a distinct optical signature upon binding to cellulose *(74, 75)*. Application of h-FTAA on native *Salmonella* spp biofilms, which contain cellulose as ECM component *(76)*, generated a cellulose-specific fluorescent spectrum with an excitation peak at 480 nm *(74)*. This ability to rapidly detect cellulose in its native form, together with minimal sample preparation and instrumentation requirements *(74)*, could make h-FTAA a suitable candidate for diagnosis of biofilm-associated infections. Besides *Salmonella* spp, *Escherichia coli* (*E. coli*), the most common pathogen in UTI, also contains cellulose as one of its main biofilm ECM components *(76)*. It has been suggested that biofilm may be present in UTI, especially in patients suffering from recurrent infections *(77–79)*. Accumulating evidence from animal studies have also shown a biofilm-like phenotype in the proximal tubule of the nephrons *(42)* and biofilm-like aggregates in intracellular bacterial communities of the prostate glands *(80)* and the superficial cells of the bladder *(81)*, as well as biofilm-like aggregates in urine from UTI patients *(82, 83)*. As all this evidence is based on morphological observations, application of h-FTAA could help consolidate a link between UTI and biofilm.

1.3 THE DIAGNOSTIC WORKFLOW OF URINARY TRACT INFECTIONS

One of the main contributors to antibiotic resistance is the inappropriate prescription of antibiotics *(84)*. This problem mainly stems from untimely diagnosis of antibiotic resistance. In the review on antimicrobial resistance, *Tackling drug-resistant infections globally: Final Report and Recommendations*, Jim O'Neill wrote:

> I find it incredible that doctors must still prescribe antibiotics based only on their immediate assessment of a patient's symptoms, just like they used to when antibiotics first entered common use in the 1950s. When a test is used to confirm the diagnosis it is often based on a slow technology that hasn't changed significantly since the 1860s. *(5)*

Indeed, in a non-life-threatening scenario, an antibiotic prescription may be based only on clinical symptoms, without further diagnostics. In a life-threatening scenario, clinicians will also proceed to an empirical prescription of broad-spectrum antibiotics to secure a patient's life, while waiting for diagnostics to be completed *(5)*. Upon completion of diagnostics, they can opt for targeted antibiotic therapy. Both routes to treatment, however, expose patients to suboptimal or unnecessary treatment, which contributes to the emergence of resistant bacteria *(85)*. Several reports on antibiotic resistance unanimously agree that this issue can only be resolved with better and faster diagnostic methods *(3, 5, 86)*.

The diagnostic workflow in a clinical microbiology laboratory varies depending on the patient sample, type of infection and laboratory equipment. To fully characterize the disease-causing pathogen, several steps are required, which unavoidably results in long turnaround times. The following sections present an overview of the 3 main steps in a standard diagnostic workflow for UTI: bacteriuria screening, pathogen identification, and antibiotic susceptibility testing (AST) (Fig. 2) *(87)*.

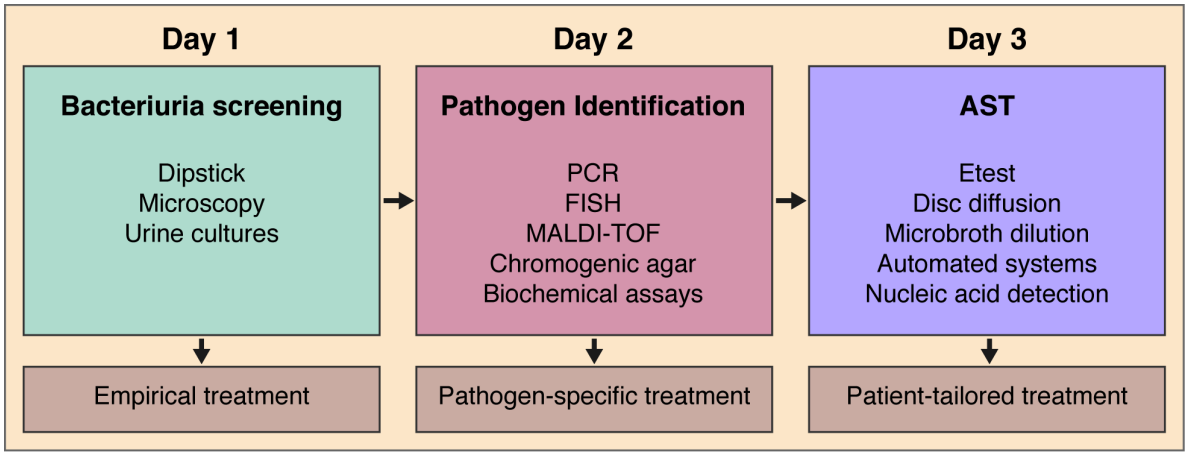

Fig. 2 Diagnostic workflow of UTI. Methods used in each diagnostic step are illustrated. The level of antibiotic treatment specificity achieved after each diagnostic step is also shown (brown box).

1.3.1 Bacteriuria screening

Laboratory testing for UTI is performed for patients experiencing symptoms, such as dysuria, urgency, and frequency *(88)*. The first step in laboratory testing is to confirm or rule out a UTI by screening for bacteriuria (Fig. 2). The gold standard to screen for bacteriuria are urine cultures on agar plates, which determine the bacterial load in urine *(88)*. Growth of a single or predominant uropathogenic species at a concentration of $\geq 1 \times 10^3$ cfu/ml indicates UTI in symptomatic patients *(88)*. Although quantitative, urine cultures require at least 18-20 h incubation before a UTI can be ruled out *(89)*. Therefore, rapid screening methods for bacteriuria are needed to avoid unnecessary prescription of antibiotics in patients without a UTI, but also to avoid unnecessary workload and costs. A rapid alternative to urine cultures is the urine dipstick, which detects a UTI based on the presence of nitrites and leukocyte esterases. Despite high specificity, sensitivity can be as low as 43.2 %, depending on the patient cohort *(90)*. As only *Enterobacteriaceae* convert nitrate to nitrite, the dipstick fails to detect other uropathogens. Moreover, urine samples can be dilute, especially in small children where frequent urination results in nitrite concentration below the limit of detection *(90)*. Microscopic analysis of Gram-stained urine samples is an alternative way to screen directly for bacteriuria. However, sensitivity and specificity greatly vary *(89)*, and it is a more laborious approach compared to the dipstick.

1.3.2 Pathogen identification

A UTI is confirmed when a patient presents both clinical symptoms and bacteriuria. However, identification of the pathogen species and subsequent antibiotic susceptibility testing are still required to avoid a prescription of antibiotics based solely on empirical assessment (Fig. 2). Current methods available for pathogen identification are matrix-assisted laser desorption/ionization time-of-flight mass spectrometry (MALDI-TOF), FISH, multiplex PCR and automated biochemical assays *(87)*. Although these assays are rapid, they require a pure bacterial culture for optimal performance. Therefore, plating of a urine culture on agar plates is required to isolate bacteria, which adds 18-20 h to the diagnostic workflow *(87)*. Identification of certain species can take place simultaneously if chromoagar is used *(91)*.

1.3.3 Antibiotic susceptibility testing

Pathogen identification can guide the clinician to select a species-specific antibiotic based on the local antibiogram. A patient-tailored antibiotic therapy, however, can only be designed by performing AST (Fig 2). In a typical AST, a standardized inoculum of 5×10^5 cfu/ml from the isolated pathogen is tested in growth media containing a 2-fold serial dilution of an antibiotic *(92)*. After overnight incubation, each antibiotic dilution is evaluated for bacterial growth using visual or instrument-assisted detection. The lowest concentration that completely inhibits bacteria from growing is defined as minimum inhibitory concentration (MIC) *(92)*. By comparing the MIC to the established clinical breakpoints for that particular antibiotic-pathogen combination, the pathogen is classified as resistant, intermediate or susceptible. Despite the great value of AST, the turnaround time of current methods exceeds

1 day. This long turnaround time is mainly affected by 3 parameters: i) the requirement for a pure bacterial inoculum of a standard concentration ii) the method's sensitivity to detect bacterial growth, and iii) the lag phase of bacteria. In the following sections, we assess AST technologies used in the clinics based on their performance for the first 2 parameters.

1.3.3.1 Antibiotic susceptibility testing directly in urine

AST is optimal when a pure bacterial inoculum of a defined concentration is used. For UTI this means that an 18-h urine culture step for pathogen isolation precedes AST *(93)*. Official guidelines discourage the direct use of urine as inoculum for AST because it can affect bacterial growth kinetics and lead to misinterpretations *(94)*. Urine has a non-standardized consistency, which varies significantly between patients in terms of pH, electrolyte concentration and other substances, such as antimicrobials *(87)(94)*. It may also contain more than one bacterial species, either due to a polymicrobial infection or contamination by microflora *(94)*. Several host components in urine, such as erythrocytes, white blood cells, and epithelial cells, can also compromise the performance of AST *(95)*. Finally, contrary to the standardized inoculum of pure cultures, the bacterial load in urine may be insufficient to perform AST directly, as shown with disc diffusion testing *(96)*.

Accordingly, there are no clinically validated methods for direct AST in urine. One promising approach is the addition of urine from a UTI patient in an excess volume of culture media containing antibiotics *(97, 98)*. An alternative approach is the sequential filtration of urine using 2 filters with different pore sizes to filter out white blood cells and large debris, but to retain bacteria *(95)*. However, the authors reported that filter clogging could be an issue. Moreover, bacteria had to be counted manually with phase-contrast microscopy to adjust their concentration before AST. Gel electrofiltration, which is integrated into the automated system Accelerate Pheno™, has been used to successfully isolate bacteria from blood cultures based on size and charge *(99, 100)*. This approach isolates bacteria from smaller contaminating substances in a sample, such as salts, proteins, and cellular debris sample, but not from larger particles, such as other contaminating bacteria or host cells *(101)*.

1.3.3.2 Antibiotic susceptibility testing based on naked eye inspection

In several of the most widely used AST methods, such as disc diffusion, Etest and broth dilution, bacteria's antibiotic susceptibility is determined by naked eye inspection at the incubation endpoint *(93)*. A long incubation time of 16-20 h is required for bacteria to reach growth levels visible to the unaided eye. In disc diffusion, a paper disc is impregnated with a single antibiotic concentration, which diffuses radially around the disc when placed on an agar plate inoculated with 1-2 x 10^8 cfu/ml of bacteria *(102)*. Inhibition of bacterial growth leaves a clear zone around the disc. Depending on the diameter of the inhibition zone, the pathogen's antibiotic susceptibility is determined. The method's throughput is low to medium; up to 6 or 12 discs containing different antibiotics can be used simultaneously depending on the agar plate's diameter (90 or 150 mm). Although cost-affordable and simple, disc diffusion is only qualitative.

Etest is a plastic strip impregnated with an antibiotic concentration gradient. The strip is placed on an agar plate with a bacterial inoculum of 1-2 x 10^8 cfu/ml, and the antibiotic gradient diffuses into the agar *(92)*. After overnight incubation, inhibition of bacterial growth leaves a clear ellipse-shaped zone. Based on the intersection point of the ellipse zone with the strip, the MIC is determined by naked eye observation. Although it delivers a quantitative result, Etest has a higher cost compared with disc diffusion and a low to medium throughput with 2 or 6 strips fitting per agar plate, depending on the agar plate's diameter *(92)*.

Broth dilution is the principal liquid media-based AST. In this assay, 5 x 10^5 cfu/ml of bacteria in liquid growth media are tested against a 2-fold serial antibiotic dilution in glass tubes. After overnight incubation, visible turbidity in each tube is evaluated to define the MIC *(103)*. Although this is a low-cost and quantitative approach, it is not usually performed in the diagnostic laboratory, as it is laborious and slow. An improvement of broth dilution was its adaptation to a 96-well plate *(104)*. In this format, called microbroth dilution, volume was reduced from milli- to microliters (≈100-150 µl/well), and throughput was increased to simultaneous testing of 12 antibiotics, with eight 2-fold serial dilutions from each. After overnight incubation, the bottom of each well is examined with the help of a mirror for a visible bacterial pellet to determine a MIC.

1.3.3.3 Absorbance-based antibiotic susceptibility testing

Absorbance-based detection is more sensitive than the unaided eye, with a bacterial growth detection limit of 1 x 10^7 cfu/ml *(105)*. This limit of detection shortens the turnaround time significantly because bacteria usually reach a culture concentration of 1 x 10^7 cfu/ml earlier than 16 h. Several automated systems adopted real-time absorbance-based detection of bacterial growth in liquid media to achieve faster AST. Systems such as the MicroScan WalkAway *(106)*, BD Phoenix Automated Microbiology System *(92, 107)*, and VITEK2 *(108, 109)* have turnaround times between 4-16 h, depending on the pathogen tested. Sample loading is manual in WalkAway and BD Phoenix and automated in VITEK2 *(92)*. All 3 instruments offer improved throughput compared with conventional methods, as they run multiple tests simultaneously. WalkAway and BD Phoenix have a 96- and 84-microwell format respectively *(107)* and, VITEK2 has a 64-cubicle microfluidic cartridge *(110)*. However, only MicroScan WalkAway and BD Phoenix deliver a MIC based on true bacterial growth, as they accommodate a complete 2-fold serial dilution range for each antibiotic in their panels *(105, 111)*. VITEK2, which features only selected antibiotic concentrations, provides a MIC based on algorithmic calculations *(112)*. Overall, AST based on absorbance delivers results earlier than AST based on visual inspection but at a much higher cost.

1.3.3.4 Microscopy-based antibiotic susceptibility testing

The automated AST instrument, Accelerate Pheno™, based on dark field time-lapse microscopy, was recently approved for clinical use *(101)*. Based on microscopy, detection of bacterial growth is achieved on a single-cell level. Images of immobilized single bacteria in chambers with and without antibiotic are captured over time *(101)*. Computer-assisted

analysis of these images calculates bacterial division and deducts a growth rate based on the division frequency. By applying a machine-learning algorithm, this growth rate is compared to the growth rate of the antibiotic-free control to determine a MIC. This approach achieves a turnaround time of ≈ 7 h for Gram-negative bacteria isolated from blood *(113)*. Although rapid, the method's throughput is currently low. It can process only one sample per instrument module with the possibility to extend up to 8 modules, but at a considerable cost increase *(113)*.

1.3.3.5 Detection of antibiotic resistance with molecular diagnostics

Molecular methods based on nucleic acid detection, such as PCR, microarrays, and sequencing, identify genes or single-nucleotide polymorphisms associated with antibiotic resistance *(114–117)*. In a short turnaround time, these methods can show which antibiotics could be ineffective based on the genotypic resistance mechanism of the pathogen. Despite a positive genotypic result, the pathogen may still be phenotypically susceptible *(118)*. Therefore, a phenotypic AST is still required to confirm the genotypic result and to determine a MIC. Moreover, molecular methods are limited to pathogens with known resistance mechanisms *(118)*.

1.4 MICROBIOLOGY MEETS MICROFABRICATION

Fabrication of milli- and micrometer scale devices confer significant advantages to biology and medicine *(119)*. Miniaturized devices integrate smoothly with other instruments and sensors to develop assays with quantitative multiparametric analysis under accurately controlled *in vitro* conditions *(120)(121)*. Several miniaturized wells or channels can fit within small dimensions, dramatically increasing throughput and simultaneously decreasing reagent and sample volume requirements. These miniaturized wells and channels better match the dimensions of prokaryotic and eukaryotic cells. In combination with an optically clear material, they become suitable for single-cell analysis with microscopy and spectrophotometric detection methods *(122)*. Besides research, miniaturized devices are also ideal for clinical use as point-of-care systems at the clinician's office. All these advantages can have a substantial impact on the advancement of microbiology. Here we will discuss how bacterial pathogenesis and infection diagnostics could be benefited from the integration of microfabricated devices.

1.4.1 Towards new *in vitro* infection models

The intravital animal model for pyelonephritis enabled the study of infection with spatiotemporal resolution in its natural milieu, with intact host tissue structure and physiology *(41)*. However, animal models come with ethical and technical limitations. These include imaging depth in the tissue, exposure time and lack of resolution to image the phenotypic heterogeneity of bacteria on a single-cell level. Moreover, gene expression profiling and protein detection at the site of infection can be measured only at the infection endpoint, as this requires kidney harvesting and subsequent RNA and protein extraction. Most importantly, the host-pathogen interplay can be complicated to understand on the organ level,

and therefore reduction of the infection down to the level of single tissue or cell line using an *in vitro* model is still required.

Two-dimensional cell culture models offer great flexibility regarding handling and compatibility with analysis methods. Their setup is usually based on a well plate in which primary, cancer or immortalized epithelial cell lines from the bladder or kidney are seeded and then infected with a pathogen under static conditions *(123)*. Although cell culture models have generated a wealth of molecular data to understand the host-pathogen interactions on the renal epithelium *(124–128)*, they cannot mimic the *in vivo* complexity. The flow of the primary filtrate constantly challenges bacteria in the kidney; it is a balancing act between adhesion and discharge rather than a mere deposition of bacteria on cells as in the static environment of a well plate. Host- and bacteria-secreted factors are fluctuating rather than accumulating statically, acting locally, as well as distally, as they are transported by the filtrate flow. Moreover, cells face a primary filtrate that is continuously renewed and not saturated by bacterial and host metabolic byproducts as in well plates. Finally, the crucial parameter of shear stress, which affects renal cell's physiology and bacterial adhesion organelles, is absent *(129–134)*.

Based on advances in fluidics and microengineering, a new category of *in vitro* cell culture models was developed, called organ-on-a-chip, which recapitulates organ- and tissue-level structure and physiology *(135)*. Typically, organ-on-a-chip is based on devices with hollow microchannels seeded with cells and perfused with culture medium. Depending on the number and arrangement of microchannels, organ-on-a-chip can accommodate a single tissue or tissue interfaces. The chip format offers several advantages for a controlled, physiologically relevant *in vitro* model. Sensors, fluid flow, porous substrates and mechanical strain can be integrated to mimic organ function *(120)*. Fabrication with clear materials, such as polydimethylsiloxane, plastic, and glass, enables real-time monitoring on-chip with microscopy *(120)*. Currently, organ-on-a-chip models for several organs and tissues have been developed, such as the liver *(136–140)*, kidney *(141–145)* lung *(146, 147)*, intestine *(148, 149)* and blood-brain-barrier *(150, 151)*.

Considering all the advantages mentioned above, organ-on-a-chip would be an ideal model to study host-pathogen interactions under spatiotemporal, single-cell resolution. However, the use of organ-on-a-chip models for infection studies is still at an early stage. In a proof-of-concept study, neutrophil transmigration and phagocytosis of *E. coli* have been shown in a lung-on-a-chip containing an interface of endothelial and alveolar epithelial cells *(147)*. In a gut-on-a-chip model, co-culture of intestinal epithelial cells with an intestinal flora microbe has been achieved *(148)*. Bacterial adhesion of *Neisseria meningitidis* and *Staphylococcus aureus* to endothelial cells *(152–154)*, as well as bladder cell invasion by UPEC *(155)*, under shear stress conditions has also been explored. Microbiologists have only just unlocked the possibilities of organ-on-a-chip for infection studies. Further development of the field can lead to a better understanding of bacterial pathogenesis.

1.4.2 Phenotypic screening platforms in microbiology

Advances in genomic technologies refined our view of bacterial pathogenesis with the discovery of several new genes. Together with this explosion of genomic information, came a need for high-throughput and quantitative methods for genotypic and phenotypic screening of bacteria *(156, 157)*. Despite these needs, platforms such as the agar plate and the 96-well plates remain a staple in microbiology.

Development of the agar plate in the 1880s was instrumental in establishing causality between pathogen and disease *(158, 159)*; it enabled isolation and *in vitro* culture of bacteria from the diseased host. Today, it is considered a low-throughput platform, which generates mainly qualitative data. One major limitation is the incompatibility with spectrophotometry and microscopy. For instance, bacteria with gene mutations affecting catalytic activity can be screened only qualitatively using chromogenic or fluorogenic substrates *(160)*. Furthermore, growth is assessed at the incubation endpoint, because bacteria have to grow long enough to be visible on the macroscale. At the endpoint, only composite growth is evaluated, whereas little is revealed about gene mutations that could affect the parameters of growth rate, growth efficiency, and growth lag *(161–163)*.

The shift to liquid cultures in 96- and 384-well plates improved throughput and enabled quantitative phenotypic screening with spectrophotometry. At the same time, the large number of wells in these formats is followed by a more laborious and time-consuming sample loading that often requires automation to be robust. Moreover, well dimensions are not optimal for single-cell analysis *(164)*, especially when it comes to microscopic analysis.

An alternative to 96- and 384-well plates is the use of microfabricated devices. Several applications have already taken advantage of such devices to culture bacteria that had been uncultivable in traditional platforms and to discover new antimicrobial compounds *(165, 166)*, study bacterial behavior on a single-cell level *(167–169)*, and improve molecular methods in microbiology *(170)*. By delivering new physical techniques, microfabrication has the potential to address the need for high-throughput and high-resolution quantitative screening in microbiology, but also improve bacterial cultivation *(121, 122)*.

1.4.3 Microfabrication in antibiotic susceptibility testing

Miniaturization in clinical microbiology has the potential to improve phenotypic AST. The clinically validated automated instruments VITEK2 and Accelerate Pheno™ have already incorporated microfluidics into their system to facilitate sample loading and processing *(101, 110)*. Several other AST methods under pre-clinical development have combined microfluidics or miniaturized arrays with microscopy to determine antibiotic resistance between 2 - 6 h, either directly from a clinical sample or using a pure bacterial inoculum (Table 1) *(95, 171–175)*. Although some devices feature dozens or hundreds of miniaturized compartments, the AST throughput remains low (Table 1) *(95, 171, 172)*. The presence of only one loading inlet limits these devices to test one sample against one antibiotic concentration at a time. Without the possibility to accommodate 2-fold serial antibiotic

dilutions, a MIC cannot be determined, and therefore results are only qualitative. Besides the microfluidic design, the microscopy-based diagnosis itself limits throughput, as it is time-consuming and computationally intense for a high-throughput setting *(173)*. So far only one of these devices, based on a 96-well plate format, features dedicated inlets for each microchannel at the bottom of the wells, which enables up to 96 sample-antibiotic combinations *(173)*. However, loading of the samples is laborious; bacteria mixed with agarose are pipetted in each microchannel and after solidification, each antibiotic concentration has to be added separately. Moreover, microscopy-based detection required 20 - 30 min per sample.

Recently, a microfluidic device was combined with nucleic acid quantification to determine antibiotic susceptibility within 30 min *(98)*. An infected urine sample was mixed with culture broth and incubated for 15 min, before proceeding with digital PCR in a microfluidic device with 1280 wells. However, similar to the other AST methods described, this device contains only one loading inlet. This limits the throughput to testing one sample against one antibiotic concentration per device at a time, and therefore a MIC cannot be determined. Moreover, sample preparation for this method is rather laborious, as it includes several steps, such as heat treatments, DNA extraction, and DNA concentration adjustment.

The short turnaround times reported in these microfluidic AST methods are often based on either a few bacterial strains or a limited number of antibiotics (Table 1) *(95, 98, 171, 172, 174)*. Testing with an extended number of strain-antibiotic combinations would most likely reveal a considerable variability in turnaround time, considering the heterogeneity among bacteria, as well as the different mode of action of each antibiotic. Considering the advantages and disadvantages of these studies, future efforts should focus on the development of a miniaturized AST that is rapid, high-throughput, quantitative and user-friendly.

Table 1. Comparison of microfabricated AST methods

	Method characteristics							
	Direct AST[1]	**Turnaround time**	**Detection method**	**Design**	**Sample throughput[2] (n)**	**[AB] throughput[3] (n)**	**MIC**	**Samples tested**
Lu, 2013 *(171)*	Yes[4]	2 h[5]	Phase-contrast microscopy	68 channels	1	1	No	2 strains (UPEC)
Baltekin, 2017 *(172)*	No	2 h 10 min[6]	Phase-contrast microscopy	2000 cell traps	1	1	No	49 strains (UPEC)
Choi, 2014 *(173)*	No	3-4 h	Bright-field microscopy	96 wells	96	96	Yes	189 strains (multiple species)
Hou, 2014 *(174)*	No	3 h 45 min[7]	Phase-contrast microscopy	1 channel	1	1[8]	Yes	3 strains (3 species)
Matsumoto, 2016 *(175)*	No	3 h	Phase-contrast microscopy	5 channels	5	3	No	101 strains (*P. aeruginosa)*
Avesar, 2017 *(95)*	Yes	5-6 h[9]	Fluorescence microscopy	200 arrays	1	1	No	5 UTI urine samples
Schoepp, 2017 *(98)*	Yes	≈ 30 min	Digital PCR	1280 wells	1	1	No	51 UTI urine samples

[1]Direct application of infected urine as inoculum for AST
[2]Number of samples loaded simultaneously in one device
[3]Maximum number of antibiotic concentrations [AB] loaded simultaneously in one device
[4]Spiked urine
[5]1 h sample pre-incubation + 1 h AST
[6]2 h sample pre-incubation + 10 min AST
[7]1h 15 min device preparation + 2 h 30 min AST
[8]Antibiotic gradient
[9]30 min preparation + 4 h 30 min - 5 h 30 min AST

2 AIMS

Advances in the field of microfabrication and organic chemistry can revolutionize the study of bacterial pathogenesis and address unmet needs in clinical diagnostics. In my thesis, I worked at the intersection of microbiology, miniaturized devices, and optical probes to:

1. Develop a rapid and high-throughput AST method
2. Establish a high-resolution phenotypic screening platform for bacteria
3. Delineate UPEC pathogenesis in pyelonephritis with a temporal and single-cell resolution by simulating the proximal tubule physiology *in vitro*
4. Develop a diagnostic method for biofilm-associated UTI based on the detection of cellulose as a biofilm marker

3 RESULTS AND DISCUSSION

3.1 THE NANOWELL SLIDE AS A NEW PLATFORM FOR MICROBIOLOGY

Papers I-III describe the development of clinical and research applications for microbiology using a nanotiter well plate. This miniaturized plate called the nanowell slide (nwSlide), features 672 nanotiter wells (nanowells) within the dimensions of a microscope slide (25 x 75 mm) (Fig. 3A, B) *(176)*. It comprises a 500-µm thick silicon grid anodically bonded to a 175-µm thick glass slide (Fig. 3C). This grid is designed in an array of 14 rows x 48 columns, which forms the 672 nanowells when bonded to the glass slide. Each nanowell has outward-tilted walls with a surface area of 650 x 650 μm^2 at the bottom and 1360 x 1360 μm^2 at the top, generating a 500-nl volume capacity per nanowell (Fig. 3C). The design and material of the nwSlide offer several advantages for microbiology. The glass bottom and slide dimensions allow for high-resolution microscopy. The inter-well distance is small enough to maximize the nanowell density on the slide but at the same time compatible with mainstream lab instrumentation, such as fluorescence activated cell sorting (FACS) and spectrophotometry *(177)*. The nanowell volume capacity of 500 nl dramatically decreases reagent consumption down to ≈336 µl. In contrast to other high-throughput well plates, where automated liquid handling is needed due to their considerable well height, the 675-µm thickness of the nwSlide enables manual loading in a single pipetting step. In papers I-III we leveraged the versatility of the nwSlide to develop a rapid, high-throughput AST and a multiparametric phenotypic screening platform for bacterial mutants.

3.2 PAPER I: DEVELOPMENT OF A RAPID ANTIBIOTIC SUSCEPTIBILITY TESTING METHOD ON THE NANOWELL SLIDE

Paper I reports our first steps in transforming the nwSlide into a nanowell AST method (nwAST). First, we designed and tested the procedures for antibiotic coating and bacterial sample loading. We coated the nwSlide with seven 2-fold serial dilutions of ampicillin, spanning a clinically relevant range between 0.5 – 32 µg/ml (Fig 3D). To allow for technical replicates, which are usually absent in clinical AST, each dilution was coated in 35 nanowells. To evaluate the quality of each test, 2 areas were designated to control for reagent contamination (negative control) and sample loading (positive control). The slim design of the nwSlide enabled us to easily load bacterial samples by smearing. The nwSlide was then sealed with a gas permeable PDMS membrane. To enable detection of growth during incubation at 37°C, we applied absorbance recordings. We adapted the nwSlide for use with a well plate spectrophotometer by fitting it in a custom 3D-printed adapter with the dimensions of a 96-well plate (Fig. 3E). By introducing all these adjustments, the nwSlide was transformed into a phenotypic nwAST.

We evaluated technical performance by inoculating the nwAST with 1×10^5 cfu/ml (50 cfu/nanowell) of the reference *E. coli* strain ATCC 25922. While incubating the nwAST in the spectrophotometer at 37°C, we measured absorbance every 10 min for 10 h. Because of the multitude of nanowells on the slide, visualization and interpretation of kinetic absorbance

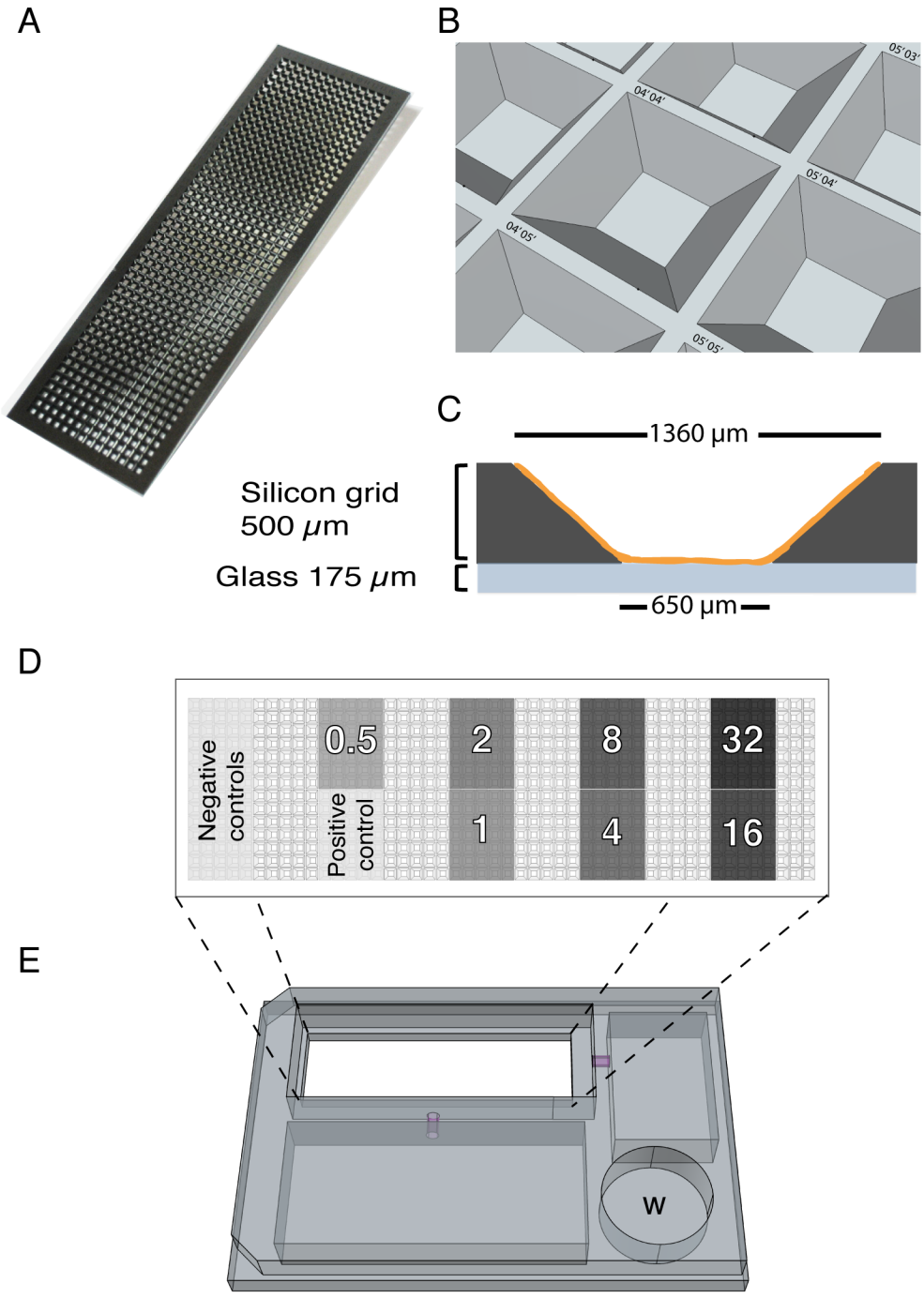

Fig. 3 Illustration of the nwAST. (A) Top view of the nwSlide and **(B)** a close-up of individual nanowells. **(C)** Side view of a nanowell with antibiotic coating (orange). **(D)** Layout of the nwAST functionalized with a 2-fold serial dilution of ampicillin between 0.5 – 32 µg/ml. Each dilution was coated in 35 nanowells. A positive (antibiotic-free) and negative (32 µg/ml ampicillin) control was included. **(E)** The custom 3-D printed adapter makes the nwSlide compatible with a well plate spectrophotometer. Dashed lines indicate the position of the nwSlide in the adapter. Screws (purple) lock the nwSlide in place. A waterbath (W) is included to prevent evaporation in the nwSlide. (Figure reprinted from Weibull E. et al., 2014).

measurements as growth curves would be a daunting task. Instead, we chose heatmaps to present a clear overview of bacterial growth under different antibiotic concentrations. Examination of the heatmap showed that growth was inhibited at ≥ 8 µg/ml of ampicillin, defining this concentration as the MIC. This result was in agreement with Etest and microbroth dilution assays, as well as the Clinical & Laboratory Standards Institute guidelines *(178)*. We concluded that antibiotic coating, sample loading, and adjustment to the 3D-printed adapter were optimally performed, demonstrating the suitability of the nwSlide for AST.

Guidelines for the interpretation of antibiotic susceptibility results are based on a standardized bacterial inoculum of 1-5 x 10^5 cfu/ml. This requires the isolation and subculture of bacteria from a patient sample before performing AST. To investigate whether the nwAST generates accurate results when the inoculum deviates from the guideline recommendations, we tested 1 x 10^4 cfu/ml (5 cfu/nanowell) and 1 x 10^6 cfu/ml (500 cfu/nanowell) of ATCC 25922 against ampicillin. We determined a MIC of 8 µg/ml regardless of the inoculum concentration. Therefore, we could accurately determine susceptibility even when there was a 10-fold deviation from the standard inoculum. This showed the potential for directly applying bacteria isolated from patient samples on the nwAST. Further investigation is needed as different inoculum concentrations, especially > 1 x 10^5 cfu/ml, can affect the MIC for several antibiotics *(179)(180)*.

It became evident from heatmaps that absorbance-based detection could differentiate between resistant and susceptible bacteria before the incubation endpoint of 10 h. Thus, we implemented an algorithm that identifies the time point (T_{lag}) when bacteria transition from lag to log phase. This algorithm processes absorbance measurements preceding and following the time point in question and determines whether absorbance has increased. If this increase exceeds a predefined threshold, this is interpreted as bacterial growth. We applied the T_{lag} algorithm on absorbance recordings from the nwAST of ATCC 25922 against ampicillin. Depending on the inoculum concentration, a $T_{lag} \approx 1 - 4$ h was found for ≤ 4 µg/ml ampicillin, whereas no T_{lag} was generated for ≥ 8 µg/ml ampicillin. Thus, the T_{lag} differentiated between inhibited and non-inhibited bacteria and determined a MIC = 8 µg/ml, which was in agreement with the analysis at the incubation endpoint. To verify the accuracy of T_{lag}, we examined bacteria in each nanowell by microscopy. We found that the T_{lag} algorithm was 98.3 % accurate, with only a few false positive and false negative nanowells for bacterial growth. Importantly, the technical replicates of the positive controls generated similar T_{lag} values, which showed that bacteria were evenly loaded on the nanowells. Because the algorithm's calculations require absorbance data from time points following the time point in question, the total turnaround time is 2 h longer than the T_{lag} calculated value. Thus, the MIC determination time for ATCC 25922 would be 3-6 h, depending on the inoculum concentration. Considering that conventional AST delivers results at 18 h, the T_{lag} algorithm shortened the turnaround time by 3-6 times.

Ideally, the nwAST should feature multiple antibiotics without the risk of cross-contamination between nanowells. To that end, we coated the nwSlide with 3 different antibiotics in adjacent areas. We added 2 concentrations from each antibiotic, one above and one below the clinical breakpoint. Testing of ATCC 25922 showed that the nwAST accurately determined the susceptibility pattern for 3 antibiotics simultaneously within 4 h 10 min, without any signs of cross-contamination.

After optimizing the parameters of nwAST with ATCC 25922, we tested whether antibiotic susceptibility could be determined using clinical UPEC isolates. For this purpose, we coated the nwSlide with 2-fold serial dilutions of ciprofloxacin and cefotaxime and loaded the nanowells with 3 clinical UPEC strains on separate slides. To reduce the turnaround time of the T_{lag} algorithm, absorbance was measured every 5 instead of 10 min. nwAST results were in agreement with Etest and VITEK2 for all 3 strains, with a turnaround time of ≈ 3-4 h. Collectively these results showed that the nwAST delivers accurate results for clinical strains up to 6 times faster compared to other clinically established AST methods.

3.3 PAPER II: CLINICAL ADAPTATION AND VALIDATION OF THE NANOWELL ANTIBIOTIC SUSCEPTIBILITY TESTING METHOD

In Paper II we adapted the nwAST to meet clinical requirements for UPEC testing. The European Committee on Antimicrobial Susceptibility Testing (EUCAST) recommends that AST for *E. coli* should be performed under aerobic conditions. We investigated the culture conditions in sealed nanowells by culturing *E. coli* WT and Δ*fnr*, a mutant with impaired growth under anaerobic conditions. This mutant exhibited a similar growth rate and culture density as the WT strain, showing that the nanowell microenvironment is aerobic for at least 16 h.

UPEC is routinely tested against 6 antibiotics at Karolinska University Hospital: ampicillin, ciprofloxacin, cefadroxil, mecillinam, nitrofurantoin, and trimethoprim. We aimed to design the nwAST so that a MIC is determined for all 6 antibiotics. MIC determination can help clinicians to optimize antibiotic therapy *(181)*. Moreover, it offers better surveillance of the infection-causing pathogen, as antibiotic treatment could still fail against susceptible bacteria that have a MIC close to the clinical breakpoint *(182)*. Therefore, we coated the nwSlide with seven 2-fold serial dilutions for each antibiotic, 2 above and 5 below the clinical breakpoint (Fig. 4). Each dilution was coated in 4 nanowells to control for technical reproducibility.

We evaluated clinical performance with 70 UPEC clinical isolates, using agar disc diffusion assays as the reference method. The overall categorical agreement was 97.9 %, which surpassed the minimum FDA requirement of 90% *(183)*. Major errors ranged between 0 - 8.3 % depending on the antibiotic, whereas no very major errors were detected. Overall, these results showed an excellent clinical performance for the nwAST when compared to agar disc diffusion.

The bacterial lag phase can range from one to several hours depending on the antibiotic-strain combination *(184, 185)*. The large number of tested UPEC gave us an excellent opportunity

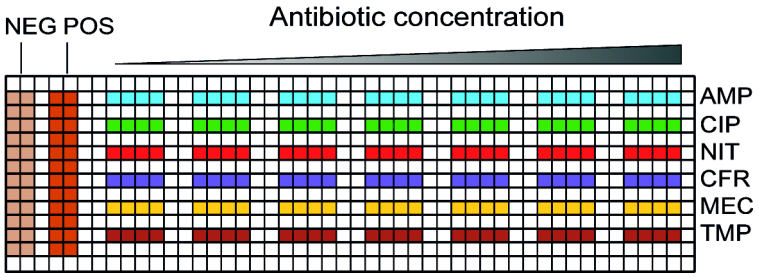

Fig. 4 nwAST layout for UTI. The nwSlide was coated with 6 antibiotics: ampicillin (AMP), ciprofloxacin (CIP), nitrofurantoin (NIT), cefadroxil (CFR), mecillinam (MEC), and trimethoprim (TMP). Seven concentrations, in 4 technical replicates each, were added from each antibiotic. Negative (NEG, medium only) and positive (POS, medium + bacteria) control areas of 24 nanowells each were also included. (Figure modified and reprinted from Veses-Garcia M. et al., 2018)

to investigate the impact of bacterial heterogeneity on diagnostic turnaround time. For resistant strains, application of the T_{lag} algorithm showed that T_{lag} ranged between 1 h 40 min - 6 h 10 min. This corresponded to an overall turnaround time of 3 h 40 min – 8 h 10 min. For susceptible strains, T_{lag} ranged between 1 h 30 min - 10 h, which corresponded to an overall turnaround time of 3 h 30 min - 12 h. These broad ranges of turnaround times reflected the biological variability of different UPEC strains. The finding that resistant bacteria transition from lag to log phase as late as 6 h 10 min post-inoculation stresses the importance of adequately incubating a sample before determining susceptibility. An incubation time shorter than a strain's lag phase could generate a very major error by misidentifying a resistant strain as susceptible. Contrary to other studies that set a predefined incubation time based on findings from a few strain-antibiotic combinations, our study highlights the advantage of using an algorithm that adapts on bacteria's lag phase.

A prolonged lag phase can delay absorbance-based detection of bacterial growth and consequently the AST turnaround time. To circumvent this type of delay, we took advantage of the nwAST's compatibility with microscopy. Depending on their mode of action, antibiotics can affect bacterial morphology *(186–190)*. To investigate whether we can determine their susceptibility based on morphology, we tested 2 UPEC strains incubated against the 6-antibiotic panel in the nwAST. After 3 h of incubation, we captured images of their morphology for each antibiotic concentration. We performed morphotyping analysis on the captured images by analyzing 3 different bacterial shape parameters: major/minor axis ratio, perimeter, and circularity. Strains susceptible to antibiotics deviated from the typical rod-shaped morphology of *E. coli*, forming filaments or exhibiting swelling. In contrast, resistant strains retained the rod-shaped morphology. This proof-of-concept investigation showed that microscopy could potentially resolve delayed diagnosis and indicate whether the lack of T_{lag} in a sample is due to true susceptibility or a prolonged lag phase.

3.4 PAPER III: THE NANOWELL SLIDE AS A PLATFORM FOR MULTIPARAMETRIC PHENOTYPIC SCREENING OF BACTERIA

In Paper III we developed the nwSlide into a phenotypic screening platform for rapid identification of growth-, metabolism-, and morphology-associated mutations in bacteria (Fig. 5). Isolation of single bacterial colonies by streaking on agar plates is a prerequisite for all downstream analyses in microbiology. We exchanged the agar plate for the nwSlide and

developed a FACS-based workflow to deposit single-bacteria in each nanowell with a labeling-free gating strategy. We evaluated this strategy by sorting a mixture of 3 flagellar mutants (Δ*fliD*, Δ*fliS,* Δ*fliT*) at a 1:1:1 ratio on the nwSlide. Bacteria were incubated and then retrieved with needles through the soft penetrable membrane of the nwSlide for downstream subculturing and mutant identification. Screening of subcultured bacteria with PCR showed a single-mutant relative frequency of 82.8 ± 7 %. Thus, we successfully obtained monoclonal cultures in the majority of the nanowells.

Algorithm-assisted analysis of absorbance measurements in Paper I & II enabled us to quickly and accurately identify nanowells with growing bacteria and determine their lag phase duration (T_{lag}). In Paper III we improved algorithm-assisted analysis by developing a 3-checkpoint algorithm, which we termed nanoculture Optical Signal Analysis Tool (nOSAT). These 3 checkpoints control: i) whether a nanowell culture generated a T_{lag}, (ii) whether it reached maximum optical density (OD_{max}) ≈ 0.006 – 0.075, and (iii) whether it exceeded growth efficiency ≥ 0.006. When absorbance measurements meet all 3 checkpoints, a nanowell is designated as a successfully grown bacterial culture. We evaluated nOSAT by processing absorbance measurements from cultures deriving from single-sorted bacteria on the nwSlide. Comparison of nOSAT with growth detection by microscopy showed 95.24 % sensitivity and 98.77 % specificity in identifying nanowells with bacterial growth. The few false negatives that affected sensitivity were due to bacterial growth levels below the detection limit of spectrophotometry. In rare cases, empty nanowells with absorbance fluctuations were designated as positive for bacterial growth, which accounts for the small number of false positives affecting specificity. Overall, we developed a robust algorithm that copes with absorbance artifacts, identifies bacterial growth, as well as determines the lag phase duration and growth efficiency in nanowells.

Phenotypic screening of bacteria usually requires initial selection of monoclonal colonies on agar plates, which are then analyzed by subculturing in microtiter plates containing colorimetric or fluorogenic substrates. We aimed to develop a one-step phenotypic screening workflow. As a proof-of-concept, we designed an assay to discriminate between *E. coli* bacteria with a positive or negative β-galactosidase phenotype. This assay was based on fluorescence emitted by the substrate 4-Methylumbelliferyl β-D-galactopyranoside (MUG) as it becomes hydrolyzed by β-galactosidase. First, we incubated separate cultures for WT and Δ*lacZ* bacteria on nwSlides loaded with MUG. We recorded fluorescence at the incubation endpoint to establish the fluorescence discrimination threshold between WT and Δ*lacZ*. To test the assay's feasibility, we added Δ*lacZ* in WT bacterial samples at a representation of 0.2, 2 and 20 % and single-sorted the mixed samples on nwSlides loaded with MUG. We were able to phenotypically identify Δ*lacZ* in the nwSlide with an accuracy ranging from 87.12-100 %, depending on its representation in the sample. These results demonstrated that our assay could detect a phenotype of interest down to 0.2 % representation in a sample in a one-step workflow.

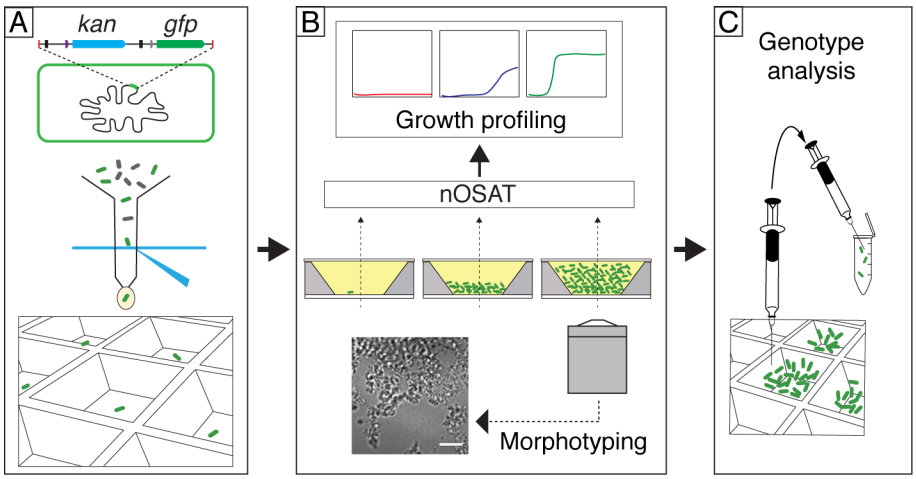

Fig. 5. A platform for multiparametric phenotypic screening of bacterial mutants on the nwSlide. (A) *E. coli* was electroporated with the TnMHA transposon, which encodes a kanamycin resistance gene and GFP. Bacteria successfully integrating TnMHA were selected based on GFP fluorescence with FACS and single-sorted on the nwSlide. **(B)** Single-sorted mutants were incubated and monitored with kinetic absorbance measurements (dotted arrows) for 16 h. Absorbance data were processed with nOSAT to determine the bacterial growth profile in each nanowell. Microscopy was applied to identify mutants deviating from normal morphology. **(C)** Based on growth and morphological profiles, mutants with phenotypes of interest were retrieved and subcultured for genotype analysis. The transposon insertion site was mapped using a cloning-free screening, comprising a single-primer PCR and sequencing. (Figure reprinted from Antypas H. et al., 2018).

Another microbiology application that could be benefited from the combination of the nwSlide with FACS is transposon mutagenesis. Therefore, we developed a one-step workflow to directly select and phenotypically screen transposon mutants. To take advantage of FACS, we constructed the transposon TnMHA, which encodes the green fluorescent protein (GFP) and kanamycin resistance (Fig. 5A). To evaluate whether FACS discriminates between WT and TnMHA mutants, we electroporated *E. coli* with TnMHA and then analyzed bacteria for GFP fluorescence in the sorter. Analysis showed a GFP-fluorescent subpopulation of bacteria, demonstrating that bacteria successfully integrated and expressed TnMHA. GFP-positive bacteria were single-sorted on a nwSlide loaded with medium containing kanamycin. In this second selection step, kanamycin prevented growth of WT bacteria that were falsely sorted on the nwSlide. After 16 h incubation with kinetic absorbance measurements, nOSAT identified 371 nanowells with successfully grown transposon mutants (Fig. 5B).

Transposons are inserted at random locations in the bacterial chromosome. Gene disruption can lead to an altered phenotype, which could help us understand gene function. Using nOSAT, we identified transposon mutants deviating from the median lag phase duration and growth efficiency. By applying microscopy, we identified a mutant forming clumps of tightly aggregated bacteria and another mutant forming highly irregular aggregates. To map the transposon insertion sites in these mutants, bacteria were retrieved from the nwSlide and screened using a cloning-free procedure, based on single-primer PCR and sequencing (Fig. 5C). Thus, by employing this workflow, a rapid first link between gene and phenotype was established.

3.5 PAPER IV: INVESTIGATION OF UROPATHOGENIC *ESCHERICHIA COLI* COLONIZATION UNDER SHEAR STRESS USING A RENAL PROXIMAL TUBULE-ON-A-CHIP

In paper IV, we developed a physiologically relevant *in vitro* model to investigate UPEC colonization in pyelonephritis. Using microfluidic channels seeded with human renal epithelial cells, we studied bacterial pathogenesis under shear stress (Fig. 6). In this model, named proximal tubule-on-a-chip (PToC), we mimicked the shear stress of the S1 segment of the proximal convoluted tubule (Fig. 6A) because it would enable to compare our results with previous findings from intravital imaging of the S1 segment in rats *(42)*. By placing PToC inside a portable 37°C incubator on the microscope stage, we were able to monitor the infection with a full temporal resolution by performing time-lapse microscopy (Fig. 6B).

Bacterial adhesion to renal epithelial cells is essential for the establishment of pyelonephritis. To study adhesion, we cultured UPEC CFT073, a pyelonephritic isolate, in cell culture medium until exponential phase. Yeast and blood agglutination showed that bacteria were expressing both P and Type 1 fimbriae under these conditions. By introducing CFT073 in PToC, the bulk of bacteria were rapidly expelled, with only a few resisting the flow. To analyze these events in more detail, we performed single-cell trajectory analysis (SCTA) on time-lapse microscopy videos recorded in the PToC. With this analysis, we tracked single bacteria in our microscopic field of view during the first 8 s of infection to characterize their displacement by the flow. SCTA identified 3 displacement patterns: 1) linear displacement with a mean velocity > 30 μm/s, 2) linear displacement with a mean velocity < 30 μm/s, 3) non-linear displacement with a mean velocity < 30 μm/s. In pattern 1, displacement was mainly dictated by the flow, and therefore bacteria were designated as unbound. In contrast, bacteria exhibiting patterns 2 and 3 were resisting the flow. We designated these bacteria as rolling and bound respectively. Although not completely immobilized on renal cells, rolling bacteria were displaced at a much slower velocity compared to unbound bacteria, suggesting that they had established weak interactions with renal cells. Bound bacteria were relatively few. They were immobilized on renal cells either briefly (< 8 s) or throughout the 8-s time-lapse video. This suggested that a minority of bacteria expressed the fimbrial profile required for initial adhesion to renal cells under shear stress.

To understand how CFT073 expands on renal cells under shear stress, we followed bacteria with SCTA throughout the first hour of infection. We observed an equal number of attachment and detachment events that resulted in a rapid turnover of adherent bacteria. Binding duration for the majority of bacteria was 1-2 min (50.2 ±11.9 %) and 2.5-30 min (42.8 ± 8.2 %). A minority (7 ± 4.8 %), however, was able to remain stably attached for longer than 30 min. We designated these bacteria as the founder population of infection. To investigate the role of fimbriae in initial adhesion, we constructed an isogenic CFT073 Δ*papG* mutant. Binding duration was significantly reduced in the absence of PapG, with 85 ± 1.6 % of Δ*papG* bacteria adhering for 1-2 min and 12 ± 4.7 % for 2.5 -30 min. Long-term adhesion of Δ*papG*, however, was not significantly different compared to WT, with

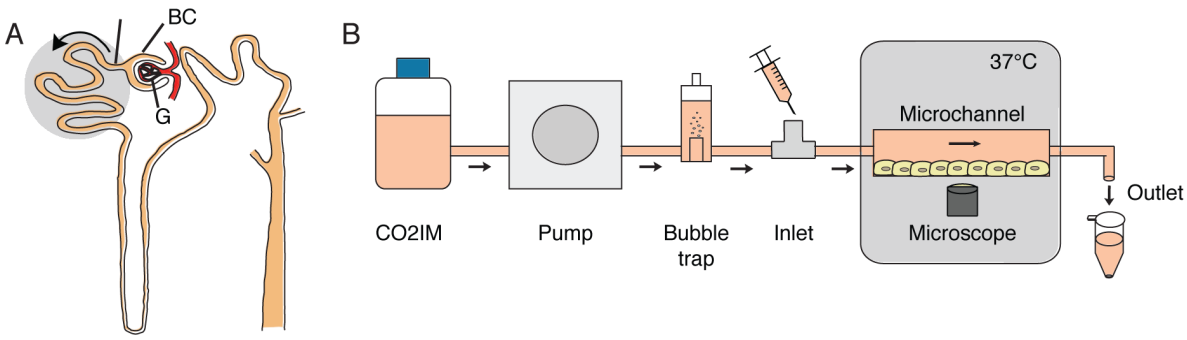

Fig. 6 Simulation of the renal proximal tubule environment *in vitro*. (A) Illustration of a nephron. Blood filtration in the glomerulus (G) generates the primary filtrate, which enters the Bowman's capsule (BC) and flows through the S1 segment of the proximal convoluted tubule (grey shade). Exposure of the renal epithelial cells to the primary filtrate flow generates shear stress on their surface. Arrow = primary filtrate flow direction. **(B)** Illustration of the PToC setup. CO2-independent medium pumped at a flow rate of 75 µl/min enters a microchannel seeded with A498 renal cells, simulating the shear stress in the S1 segment of the proximal tubule. The slide with the microchannels is placed on the microscope stage inside a portable incubator at 37°C. Bacteria are injected in the microchannel via the inlet and infection is followed with phase-contrast time-lapse microscopy.

3 ± 3.9 % adhering for longer than 30 min. Overall, PapG prolonged binding duration, but it was not essential for long-term adhesion.

We monitored the founder population of bacteria with time-lapse microscopy to understand how these few bacteria develop into an infection. Shortly after adhering to renal cells, several bacteria multiplied with a generation time of ≈ 20 min. Rapid division was crucial for overcoming detachment due to shear stress. Bacteria bound for longer than 20 min had sufficient time to divide and further establish UPEC's presence on renal cells in 2 ways. After each division, daughter cells released into the microchannel helped to spread the infection, whereas daughter cells remaining attached formed aggregates. These aggregates gave rise to microcolonies, which presented UPEC with several advantages. Firstly, microcolonies enabled bacteria to expand beyond the cell surface and form 3-dimensional microcolonies. In the *in vivo* situation, the ability to extend towards the lumen of the proximal tubule would confer a significant colonization advantage. Secondly, bacteria in microcolonies continued to proliferate rapidly, contributing to the microcolony size and infection spread by releasing an even higher number of bacteria. Thirdly, microcolonies showed increased resistance to shear stress and remained bound for several hours. These findings demonstrated how the transition from a single-cell to microcolony lifestyle consolidated UPEC's presence on renal cells under shear stress.

When we followed infection with an isogenic Δ*fimH* mutant of CFT073 in PToC, we observed that bacteria also multiplied rapidly, but expanded almost exclusively as a single layer in direct adhesion to renal cells, whereas the ability to form microcolonies was severely impaired. This suggested that FimH is involved in interbacterial interactions in pyelonephritis, which might be mediated by binding to mannose residues of LPS *(48)*. Further investigations, however, are needed to show whether the mannose-binding lectin domain of FimH is involved.

PapG and FimH enhanced the ability of UPEC to colonize renal cells under shear stress. Therefore, we investigated their role in the infection outcome. CFT073 WT was expressing both adhesins, and it was able to colonize renal cells and trigger cell rounding at ≈ 2.5 h. In contrast, the adhesin mutants required more time to colonize host cells, with Δ*papG* triggering host cell rounding after 3.5 h and Δ*fimH* after 4 h. These findings showed that the onset of host-cell rounding is proportionate to the bacterial load present on renal cells and that it is triggered regardless of the PapG and FimH presence. Despite PapG and FimH enhancing colonization, they were not a prerequisite to establish an infection. We concluded that UPEC harbors a broad repertoire of redundant fitness and virulence determinants to establish an infection under shear stress in a PapG- and FimH-independent manner. Contrary to static *in vitro* cell cultures, PToC delineated UPEC colonization with a single-cell temporal resolution under shear stress conditions.

3.6 PAPER V: DETECTION OF CELLULOSE IN URINE AS A BIOMARKER FOR BIOFILM-ASSOCIATED URINARY TRACT INFECTIONS

In Paper V, we investigated whether UTI can be biofilm-associated. Cellulose is an ECM component of UPEC biofilm, which is not naturally produced by the human host. Therefore, we aimed to screen urine from UTI patients for the presence of cellulose as a biomarker for biofilm-associated UTI. To that end, we set up a novel method named cellulose optotracing, based on the LCO h-FTAA (Fig 7A). In this method, a sample is incubated with h-FTAA for 15 min and then excited using a spectrophotometer between 300-520 nm with emission collected at 545 nm. If there is cellulose in the sample, h-FTAA changes its conformation upon binding to cellulose and generates a cellulose-specific fluorescence spectrum with a primary excitation peak at 464 nm and a secondary at 488 nm.

Cellulose forms a mesh with other proteins and polysaccharides in the ECM of UPEC biofilm *(191)*. To investigate whether optotracing detects cellulose in its native complexity, we screened biofilm from UPEC No12, which is a UTI isolate characterized as a cellulose producer based on its morphotype on Congo red agar plates *(70)*. Optotracing generated an excitation spectrum with a primary excitation peak at 464 nm and a secondary at 488 nm (Fig. 7B, red line). In contrast, cellulose optotracing of UPEC No12 Δ*bcsA*, an isogenic mutant of the cellulose synthase catalytic subunit, generated a spectrum lacking these 2 excitation peaks (Fig. 7B, blue line). These results defined the 464- and 488-nm peaks as a cellulose-specific spectral signature and showed that optotracing detects cellulose in the complex ECM of UPEC, without interference from other biofilm components.

Ideally, cellulose detection should be performed directly in urine. To characterize urine as a potential matrix for cellulose optotracing, we first characterized urine's native fluorescence. We excited urine samples from 8 healthy volunteers between 300-520 nm and collected emission at 545 nm, the same wavelength settings used in cellulose optotracing. Our results showed that urine has strong fluorescence across all wavelengths, with excitation peaks between 360 - 380 nm. Moreover, the amplitude of fluorescence greatly varied among different samples. We then investigated whether urine's native fluorescence interferes with

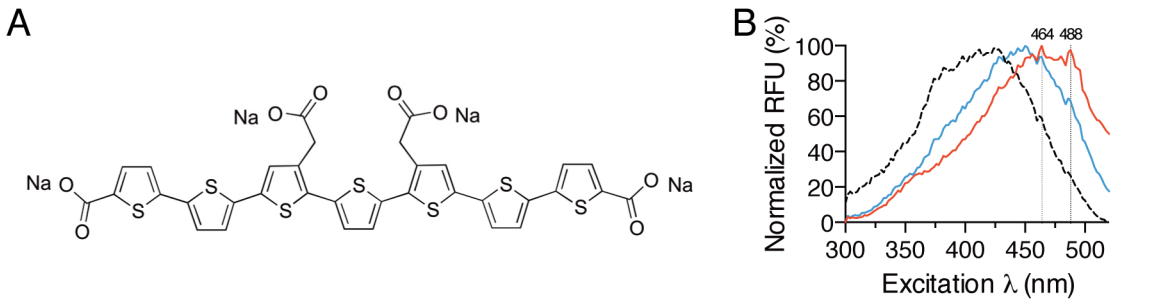

Fig. 7 Cellulose optotracing in UPEC biofilms. (A) Structure of h-FTAA. **(B)** Normalized excitation spectra of cellulose optotracing in WT (red) and Δ*bcsA* (blue) biofilms of UPEC No 12 suspended in PBS. Average normalized fluorescence from n = 3 is shown. Black line = PBS + h-FTAA; Dotted vertical lines indicate the 464- and 488-nm peaks of the cellulose spectral signature.

cellulose optotracing. We spiked 8 healthy urine samples with the same amount of purified cellulose and subjected them to optotracing. Although a clear cellulose-specific spectral signature was generated from 2 samples, urine's fluorescence dominated over the cellulose signature in the other 6 samples. We concluded that cellulose optotracing directly in urine is feasible, but the variability of urine among different individuals can affect the reproducibility of the method and generate false negative results.

Reproducibility is essential in an assay intended for clinical use. As urine was not a suitable matrix for optotracing, we replaced it with PBS. We initially spiked a healthy urine sample with WT and Δ*bcsA* UPEC biofilm and performed optotracing. Despite containing cellulose, the WT biofilm generated a negative result, with a similar spectral signature to Δ*bcsA* biofilm and to a non-spiked urine sample. To remove urine but keep biofilm components, we centrifuged all samples and resuspended them in PBS. Optotracing in PBS generated a cellulose signature for the WT sample, clearly differentiating it from the Δ*bcsA* biofilm and the non-spiked urine sample. Thus, this rapid and simple processing step removed any interference from urine and enabled us to detect cellulose.

Having established a workflow to process urine for cellulose optotracing, we next applied our method on urine samples from 182 UTI patients and 8 healthy volunteers. To facilitate analysis of the 190 spectra generated with cellulose optotracing, we applied Principal Component Analysis and k-means clustering. To help us classify the clusters as cellulose-positive and cellulose-negative, optotracing spectra from WT and Δ*bcsA* biofilm preparations were also included as references for the analysis. We identified 27 UTI samples that clustered together with the WT biofilm. Thus, we designated them as cellulose-positive. We found 83 UTI samples that clustered together with the Δ*bcsA* biofilm, thus defining them as cellulose-negative. Although these samples lacked cellulose, we cannot exclude the presence of biofilm with a different ECM composition. Interestingly, samples from healthy volunteers were located in the periphery of the cellulose-negative cluster. This showed that optotracing might also have the potential to differentiate healthy from UTI urine samples. Moreover, this showed that low amounts of bacterial contamination from other species in healthy urine did not produce false positive results. The remaining 72 UTI urine samples

belonged to a third cluster between the cellulose-positive and cellulose-negative clusters. The spectral information of these samples was insufficient for classification. Although their spectra were distinct from the ones in the cellulose-negative cluster, they did not feature a cellulose spectral signature. Whether these spectra were compromised by the presence of host components present in UTI urine samples, it remains to be investigated. Overall, we demonstrated direct detection of native cellulose for the first time in urine samples, providing solid evidence that UTI can be biofilm-associated.

4 CONCLUSIONS AND FUTURE PERSPECTIVES

4.1 PAPERS I-III: REINVENTING MICROBIOLOGY ASSAYS WITH THE NANOWELL SLIDE

By replacing the agar plate and standard well plates with the nwSlide, we delivered high-throughput, user-friendly and versatile platforms for AST and phenotypic screening of bacteria. With dimensions equal to a microscopy slide, the nwSlide surpasses in throughput all other standard platforms, with a potential to screen up to 672 conditions simultaneously (Table 2). The possibility to include 4 technical replicates of 7 dilutions from 6 antibiotics enabled both MIC detection and technical reproducibility control. The full throughput potential of the nwAST has yet to be reached. Currently, we have functionalized 168 out of 672 nanowells. With the help of automation in antibiotic coating procedures, the nwAST could further expand with the inclusion of additional antibiotics and reagents for pathogen identification.

User-friendliness is a parameter often lacking in microfabricated devices. Easy inoculation of bacterial samples is one feature that made the agar plate handy for use in AST compared to the more laborious pipetting in 96- and 384-well plates. Although a multiwell device, the slim design of nwSlide enables one-step inoculation by smearing the sample across all nanowells (Table 2). Besides easy inoculation, retrieval of bacterial samples from nanowells is also feasible. When it comes to cost-affordability, the nwSlide consumes the least amount of reagents compared to the other platforms, and it can also be reused after autoclaving.

The design of the nwSlide is compatible with mainstream technologies. Spectrophotometry and microscopy on the nwAST delivered results as early as 3 h. The compatibility of the nwSlide with FACS, spectrophotometry, and microscopy merged the steps of bacterial isolation, selection, subculturing and phenotypic screening into one and decreased hands-on time. Already from the first incubation round of single-sorted transposon mutants, phenotypic screening for growth- and morphology-associated mutations could take place. Growth screening of cultures starting with single bacteria is more robust in the ≥ 8 times smaller volume of nanowells compared to 96- and 384-well plates, as bacteria reach the absorbance detection limit of 1×10^7 cfu/ml faster (Table 2). Accordingly, the smaller bottom surface and height of the nanowells are more suitable for morphology analysis by microscopy. Overall, the applications developed on the nwSlide are easily scalable to different laboratory settings to serve basic, industrial and clinical research purposes. Potential future applications could include screening of clinical or environmental samples for pathogen surveillance or even isolation and characterization of new species. Beyond assay throughput, microbiologists need more than ever to run well-controlled experiments and export high-resolution quantitative and qualitative data. Our platform delivers high-resolution data without compromising throughput, and we foresee that microbiologists will eagerly use it for a wide range of applications.

Table 2. Comparison of the nwSlide with standard microbiology platforms

	Microbiology platforms			
	Agar plate	**96-well plate**	**384-well plate**	**nwSlide**
Dimensions				
Length x width (mm)	Ø 90 or 150	127.71 x 85.43	127.76 x 85.48	75 x 25
Height (mm)	14.5	14.1	7.5 - 14.4	0.675
Throughput[1]	1	96	384	672
One-step inoculation	Yes	No	No	Yes
Sample retrieval	Yes	Yes	Yes	Yes
Reagent consumption (ml)	0.1 - 1	4.8 - 19.2	1.5 - 55.7	0.34
Reusable	No	No	No	Yes (autoclavable)
Single-cell sorting	Yes	Yes	Yes	Yes
Quantitative growth screening	−	+	+ +	+ + +
Morphological analysis	−	+	+	+ +

[1] Number of conditions that can be tested simultaneously

Key to rapid growth detection in the nwAST was the implementation of the T_{lag} algorithm on absorbance data. This algorithm detects the time point when bacteria transition from lag to log phase, rendering unnecessary to inspect a culture for bacterial growth at the incubation endpoint. Future integration of this algorithm into spectrophotometric analysis software will enable real-time detection of antibiotic resistance as soon as bacteria start to grow. Algorithm-based real-time detection is a faster and safer option contrary to assays with pre-defined incubation time. It eliminates the long overnight incubation times, and at the same time, it adjusts to bacteria's intrinsic physiology. Pre-defining a short incubation time entails the risk to misdiagnose resistant bacteria with an extended lag phase as susceptible. This was clearly demonstrated when UPEC generated T_{lag} values within a broad time range. Besides rapid growth detection, algorithm-assisted analysis facilitated the handling of a large amount of spectrophotometric data. By applying nOSAT, we detected nanowells with growth and identified differences in growth parameters rapidly, offering quantitative information from the first incubation round.

We achieved a decrease in AST turnaround time from typically 18 h down to 3-6 h. Isolation and subculturing of bacteria from a patient sample to prepare the AST inoculum is yet another time-consuming step. Further development could focus on overriding this step and run the nwAST directly with a clinical sample. Different approaches to isolate bacteria from

urine samples, such as filtration or centrifugation, could be applied. Alternatively, an infected patient sample could be mixed with a selective broth to rule out growth of non-pathogenic microorganisms and then inoculated directly on the nwAST. Validation with 70 UPEC clinical strains demonstrated the clinical potential of the nwAST for UTI. Further validation with other species, however, is still needed to verify its broad applicability in the clinics.

4.2 PAPER IV: A QUANTITATIVE REAL-TIME VIEW OF BACTERIAL PATHOGENESIS ON A SINGLE-CELL LEVEL

We demonstrated how the field of organ-on-a-chip could revolutionize the study of bacterial pathogenesis. Infection in the PToC was in line with the principal findings of the rat intravital model, showing that we successfully mimicked *in vitro* the shear stress microenvironment of the proximal tubule. Owing to the temporal and single-cell resolution of the PToC, we were able to obtain a more refined view of bacterial colonization compared to *in vivo* experiments. Quantification of bacterial adhesion showed that only a small fraction of bacteria adhered. This adhesion was mainly transient, except for a few bacteria with long binding duration, which we termed as infection founders. PapG adhesin prolonged overall binding duration, but it was not a definitive requirement for long-term adhesion, as infection founders remained unaffected by its absence. In line with the phase variation observed for several *E. coli* adhesins *(192)*, this suggested that the fimbrial profile greatly varies within a bacterial population, with only a small portion being suitably equipped to establish adhesion to renal cells under shear stress.

Rapid proliferation of the few infection founders led to the spread of the infection but also to the formation of microcolonies. This lifestyle adaptation enabled bacteria to effectively overcome shear stress and colonize renal cells. In the *in vivo* context, this strategy would be advantageous for promoting colonization throughout the proximal tubule. During colonization, an unexpected role for FimH was shown. Besides its established role in direct adhesion to Uroplakin Ia of the urothelial plaques in the bladder, it mediated microcolony formation under shear stress, suggesting an involvement in interbacterial interactions. Although the absence of PapG or FimH adhesins slowed down the infection progression, bacteria eventually colonized host cells, causing them to round up and slough off. Taken together, these results suggested the involvement of several adhesion factors with redundant roles to secure the establishment of infection under shear stress. To further understand the complexity of adhesion to renal cells, the role of other fimbriae, such as F1C and Ygi, should be investigated *(126)(193)*.

Renal cells gradually rounded up and sloughed off, as bacterial colonization progressed. Disruption of the uroepithelium has been previously linked to the effect of the bacterial exotoxin α-hemolysin *(41)(194)*. As the PToC is an excellent platform for real-time studies, future investigations could focus on the effect of α-hemolysin on epithelial disruption and the host's immune response. Ischaemia is yet another hallmark of pyelonephritis, which is manifested in the renal vasculature surrounding the infected proximal tubule *(195, 196)*. Ischaemia develops early during infection when bacteria are still contained within the

proximal tubule with no direct contact with the endothelium, suggesting a molecular crosstalk between epithelium and endothelium. Addition of a second channel to PToC would enable us to create an endothelial-epithelial interface to study the molecular crosstalk that triggers blood clotting in the vasculature surrounding the infection site. As the field is moving towards a body-on-a-chip *(197)*, connection of other organ-on-chips, such as the spleen *(198)*, will elucidate the inter-organ communication during pyelonephritis and provide the complete picture of the pathophysiology of pyelonephritis.

The development of novel *in vitro* models aims not only to increase understanding of bacterial pathogenesis but also to improve animal welfare in research. The main objectives of the "Three Rs" principles are to develop methods that replace, reduce and refine the use of experimental animal models *(199)*. Here we demonstrated that organ-on-a-chip has the potential to reduce and replace animal use in research. Simulating the *in vivo* environment on a chip creates a credible platform to thoroughly test scientific hypotheses before performing animal experiments. With the addition of several tissue components and sensors, organ-on-a-chip models have the potential to minimize or even replace the use of experimental animals.

4.3 PAPER V: ESTABLISHING A LINK BETWEEN URINARY TRACT INFECTIONS AND BIOFILM

We developed the first diagnostic assay for biofilm-associated infections based on cellulose optotracing. We demonstrated that UPEC adapts to a biofilm lifestyle as the bacteria colonize the urinary tract. As biofilm-associated infections can be hard to eradicate, it remains to be investigated whether failure of antibiotic treatment and recurrence of UTI are linked to biofilm. In contrast to laborious microscopy-based methods, in which interpretation of results is often subjective, optotracing delivers definitive cellulose detection in less than an hour, and it can be easily integrated into a clinical setting. Optotracing could also be applied for bacteriuria screening, based on its potential to differentiate between healthy and non-healthy urine. Ultimately, our diagnostic assay could help clinicians obtain a better clinical picture of the patient in order to choose an appropriate antibiotic therapy.

As this is a proof-of-concept study, there are several additional steps to take before implementing this assay in the clinics. Improvement of urine processing to selectively isolate ECM from other host and bacterial components may increase the detection sensitivity of the assay. Moreover, the ECM of UPEC's biofilm may also be without cellulose, which would go undetected by the current assay. Therefore, further screening of other LCOs could identify molecules to target additional ECM components and develop a multiplex biofilm-screening assay. Currently, there are no clinically established methods to detect cellulose, and therefore it was not possible to use a "gold standard" to describe the diagnostic accuracy of cellulose optotracing in urine. Other analytical methods may have to be explored. Contrary to the non-disruptive nature of optotracing, however, these methods detect glucose, the building blocks of cellulose *(200)(201)*. Taking into account the complexity and variability of a UTI urine sample, it would be difficult to establish such a reference method as glucose could also derive from other bacterial and host components.

5 MY CONTRIBUTION TO THE FIELD

Although the field of microfabrication has generated a plethora of new devices with improved functions and design, they are largely underused in microbiology. In my thesis I bridged, microbiology with microfabricated devices to address pressing issues in infection biology. By integrating the nwSlide into my research, I tremendously increased throughput for both AST and phenotypic screening. In parallel, a line of new tools for research and diagnostics was developed, from algorithmic and heatmap analysis to a dual selection transposon and a one-step mutant phenotypic screening. My work also examined bacterial pathogenesis on a single-cell level with full-temporal resolution, showing the potential of the organ-on-a-chip concept for infection studies. By working at the intersection of LCO and microbiology, I also developed the first diagnostic tool for biofilm-associated UTI. Biofilm detection combined with AST could provide invaluable information to clinicians and help shape future strategies for biofilm-associated infection treatment. I hope that the papers comprising this thesis clearly show the value of working at the intersection of different disciplines.

6 ACKNOWLEDGEMENTS

As a PhD-student at the Swedish Medical Nanoscience Center, I had the privilege to work with an extraordinary group of people. Without their care and support, I would not have been able to complete this thesis. I owe you all a debt of gratitude.

To my supervisor, Professor **Agneta Richter-Dahlfors**. Your dedication, support, and constructive criticism nurtured me into an independent interdisciplinary scientist. What I achieved in this thesis was far beyond what I could ever imagine, and I owe it to you. Thank you for seeing potential in me!

I am also grateful to my co-supervisor, Professor **Mikael Rhen**, for his tremendous scientific input and troubleshooting advice throughout these years. Nobody knows microbiology as you do! My deepest gratitude to the "heart of the Center", **Margret Wahlström,** for always taking care of me and for lifting me up with her kind words. To Assistant Professor **Keira Melican**, for all her support and positive energy, and for her amazing work on pyelonephritis, which inspired part of my thesis. To Assistant Professor **Susanne Löffler**, for always saving the day! You have my gratitude for being the voice of reason throughout these years, for teaching me that "life is not a fairy tale" and that PEDOT is not just "a plastic".

To my "partner in crime", **Marta Veses-Garcia**, for screening 150528 nanowells, 672 at a time. Completion of this thesis would have been impossible without your hard work! Thank you for putting up with my demanding personality and after-hours emails, for filling the lab with your laughter and my computer screen with unicorn stickers, and most of all, for being a friend. Go team "Marta-Haris"!

To the multitalented **Anette Schulz**: You were always there to give me advice, baked goods, silence, plants, a hug, and an occasional lecture on why recycling plastic bottles is important. Thank you for your kind heart, selflessness and friendship! To my eternal cheerleader, personal statistician, *lepa ženska* and friend, **Karen Butina.** Your presence in my life resulted in a highly significant increase in happiness ($P = 0.00053$). However, no significant increase in my desire to go hiking was ever observed ($P = 0.152$) despite your best efforts. Thank you for your constant encouragement and for joining me in this life adventure called KLARA! To the best office mate ever, **Sara Fahlén**. I will always cherish the fun moments we shared together in the amazing office B1-418 or should I say the *coolest* office in the whole of Neuro Department? (I know this statement may cause the envy of Susie and Ben, but a fact is a fact). Thank you for your incredible team spirit and unmatched organizational skills! To the indefatigable **Svava Steiner**. You set an example with your work ethic, generosity, and attentiveness. You have my gratitude for our stimulating discussions and for being the go-to person to answer all my clinical questions. Thank you for always having my back!

Shout-out to science influencer **@BenLibberton**! Thank you for transmitting your passion for science communication, for launching my career as a hand model, and for being the co-inventor of the Salad Mask! Special thanks to the *increíble microbiólogo,* **Jonatan**

Martín-Rodriguez, for his technical and moral support through the difficult times of lambda red recombineering. To **Ferdinand Choong**, for all his insightful comments and support over the years.

My sincere thanks to **Thomas Simonet** for his contributions to my projects. It was a joy to supervise such a smart and hard-working student! Many thanks to the other incredible past students, **Lisanne de Vor**, **Charbel Kreidy**, **Nanna Sjöstrand**, **Muriel Freixanet Gustà**, and **Delia-Maria Goilo** for boosting the fun and creative atmosphere of the Center.

Many thanks to other past members of the Center for their help: **Salvador Carretero-Gomez**, **Olga Chuquimia Flores**, **Peter Kjäll**, **Klas Udekwu**, **Gunilla Jacobson**, **Monica Rydén Aulin**, and **Karin Larsson**.

I would also like to take this opportunity to express my gratitude to our external collaborators, Professor **Annelie Brauner** at Karolinska University Hospital & MTC and Professor **Helene Andersson-Svahn** at KTH, for our fruitful collaboration, which made this thesis truly interdisciplinary! To my excellent collaborator at KTH, **Emilie Weibull**, for giving me the best possible start in my doctoral studies and for "luring" me into the world of the nanowell slide. To **Jaromir Mikes** at SciLifeLab, for his invaluable help in sorting single bacteria on the nanowell slide.

In life I chose a biofilm over a planktonic lifestyle. Like a bacterium in a biofilm, I owe my perseverance to my friends and family for being the other bacteria and extracellular matrix to embed myself into (Hint: If you don't get this, it means you skipped directly to the acknowledgement page. Go back and read the whole thesis!).

I would like to express my gratitude to **Nikos Giannopoulos**, for being an example of success and discipline in my life, for encouraging me to study hard and party even harder. Thank God I learned a few tricks about this organ-on-a-chip technology and I can make us two spare livers now! To **Athina Tzavara**, for being a constant source of positive energy in my life, for singing and dancing with me on our way to school between Panormou-Ambelokipi stations, and for being a role model of style and grace, bright as h-FTAA when bound to cellulose. To **Vasilis Tsotras**, for always being his outrageous self and blessing me with his charisma, uniqueness, nerve and talent. You had me at "*TI KOITAΣ;;;*" Sorry for stealing your thunder and planning my dissertation party on your birthday (not really). To the eternal optimist, **Aspasia Mitropoulou**, for teaching me the importance of #treatyourself, aka "*κάνε ένα δώρο στον εαυτό σου*", and for all the beautiful carefree moments during our Bachelor's programme.

Microfabrication not only delivered cool devices for my thesis, but it also delivered one of my best friends, **Yorgos Voulgaris**. Within only 1.64 cm, I never thought I could find so much love and support! Thank you for being by my side through thick and thin, you are like a brother to me! To my Greek lab soulmates, **Maria Georganaki** and **Marika Mokou**: Your encouragement during my first steps in the lab meant the world to me! Thank you for all the

pranks, the lab trolley rides, and music, for going through the trash with me to find that aqueous phase with the plasmid, and for the occasional splash of orange colour. The late Hettich Universal 16R centrifuge would have been proud of us! To **Marios Stavrou**, for his love and support since the beginning of my journey in science, and for all the Sunday afternoons with pancakes and Aperol Spritz. Thank you for creating some of my happiest moments!

Being late is not the greatest quality of mine, but it became the opportunity to meet one of my dearest friends, **Teresa Fernandez Zafra**. On the 31st of August 2010, I barely caught that bus ride to Solvik. Full bus, only one empty seat next to you, the rest is history. Thank you from the bottom of my heart for all the love, safety and comfort you gave me all these years in Sweden. A big thank you to my other amazing friends from the Master's programme, **Milind Nigam, Ioanna M. Kritikou, Luisa Hugerth, Johanna Holm** and **Susann Sandström**. You were the first people to make me feel at home in Stockholm! Thank you for all the fun moments we shared! My sincere gratitude to **Roman Rogozhnikov**, for being the driving force to wrap up my doctoral studies. I could not bear the thought of you asking me for the millionth time "When are you planning to finish with your PhD?" To my friend and part-time ex-roommate, **Dimitris Masvoulas**, for making me wake up before 8 o'clock, even if only for a short period of my life, and for making sure I practice my speaking skills in Swedish; "*men ursäkta mig*!" To **Alexandros Rammos**, for encouraging me to pursue my dreams abroad. **Antigoni Stavridou, Kelly Kollia, Antonis Karapetrides**: Thank you for making every holiday in Athens so special!

To my friend and best roommate ever, **Yannis Karachristos**. You kept me sane (and sometimes drove me insane) during one of the most work-intensive years of my life. Thank you for all your love, support, and laughter, for the Friday evenings with RPDR, *linschips*, and *proteinglass*, and for making sure we never run out of ice! You are amazing, "*okurrr*"?

To **Iraklis Papaeracleous**: You have my gratitude for putting up with my endless chatter about my thesis and manuscripts – although I am still not sure if you can tell the difference between bacteria and viruses. Thank you for brightening up the last year of my PhD with your presence, for causing micro- and nanodrama (microfabrication is everywhere!), and for always being so caring and supportive. "*Prrr*"!

To my beloved twin siblings, **Matina Antypa** and **Stavros Antypas**: You are the best thing that ever happened to me! Thank you for gracing my life with your presence – except that time you set my favourite jacket on fire. Not cool! I would also like to express my gratitude to my brother, **Spyros Antypas**, for his love and support. Thank you for being respectful when I was trying to study! My deepest gratitude to my father, **Konstantinos Antypas,** for encouraging me every step of the way, and for being my biggest supporter since day one! Thank you for raising the bar high and always pushing me to excel. To my mother, **Paraskevi Antypa**, for teaching me the most important qualities in life: kindness, selflessness, and compassion. Thank you for loving and supporting me unconditionally, for seeing me for who I am, for giving me everything! I love you!

7 REFERENCES

1. A. Fleming, On the antibacterial action of cultures of a penicillium, with special reference to their use in the isolation of B. influenzae, *Br. J. Exp. Pathol.* **10**, 226–236 (1929).

2. J. Davies, Where have all the antibiotics gone?, *Can. J. Infect. Dis. Med. Microbiol.* **17**, 287–290 (2006).

3. US Centers for Disease Control and Prevention, Antibiotic resistance threats in the United States, 2013, (2013) (available at www.cdc.gov/drugresistance/threat-report-2013).

4. ECDC/EMEA Joint Technical Report, The bacterial challenge : time to react, (2009) (available at ecdc.europa.eu/en/publications/Publications/0909_TER_The_Bacterial_Challenge_Time_to_React.pdf).

5. J. O'Neill, Tackling drug-resistant infections globally: Final Report and Recommendations, (2016) (available at amr-review.org/sites/default/files/160518_Final paper_with cover.pdf).

6. M. J. Renwick, V. Simpkin, E. Mossialos, Targeting innovation in antibiotic drug discovery and development. The need for a One Health – One Europe – One World Framework, *Heal. policy Ser.* (2016) (available at www.euro.who.int/__data/assets/pdf_file/0003/315309/Targeting-innovation-antibiotic-drug-d-and-d-2016.pdf).

7. A. Fleming, Nobel Lecture: Penicillin, (1945) (available at www.nobelprize.org/nobel_prizes/medicine/laureates/1945/fleming-lecture.pdf).

8. R. Laxminarayan, A. Duse, C. Wattal, A. K. M. Zaidi, H. F. L. Wertheim, N. Sumpradit, E. Vlieghe, G. L. Hara, I. M. Gould, H. Goossens, C. Greko, A. D. So, M. Bigdeli, G. Tomson, W. Woodhouse, E. Ombaka, A. Q. Peralta, F. N. Qamar, F. Mir, S. Kariuki, Z. A. Bhutta, A. Coates, R. Bergstrom, G. D. Wright, E. D. Brown, O. Cars, Antibiotic resistance-the need for global solutions, *Lancet Infect. Dis.* **13**, 1057–1098 (2013).

9. J. R. Porter, Antony van Leeuwenhoek: tercentenary of his discovery of bacteria, *Bacteriol. Rev.* **40**, 260–269 (1976).

10. S. M. Blevins, M. S. Bronze, Robert Koch and the "golden age" of bacteriology, *Int. J. Infect. Dis.* **14**, 744–751 (2010).

11. R. Koch, Die Aetiologie der Tuberkulose, *Mittheilungen aus dem Kaiserlichen Gesundheitsamte* **2**, 1–88 (1884).

12. B. A. Wilson, A. A. Salyers, D. D. Whitt, M. E. Winkler, *Bacterial Pathogenesis: A molecular approach* (ASM Press, Washington, DC, ed. 3rd, 2011).

13. S. Falkow, Molecular Koch's postulates applied to bacterial pathogenicity — a personal recollection 15 years later, *Nat. Rev. Microbiol.* **2**, 67–72 (2004).

14. A. S. Evans, Causation and disease: Effect of technology on postulates of causation, *Yale J. Biol. Med.* **64**, 513–528 (1991).

15. A. Casadevall, L. Pirofski, Host-pathogen interactions: Redefining the basic concepts of virulence and pathogenicity, *Infect. Immun.* **67**, 3703–3713 (1999).

16. A. Casadevall, L. Pirofski, Host-pathogen interactions: The attributes of virulence, *J. Infect. Dis.* **184**, 337–344 (2001).

17. A. Richter-Dahlfors, M. Rhen, K. Udekwu, Tissue microbiology provides a coherent picture of infection, *Curr. Opin. Microbiol.* **15**, 15–22 (2012).

18. G. R. Nielubowicz, H. L. T. Mobley, Host-pathogen interactions in urinary tract infection, *Nat. Rev. Urol.* **7**, 430–441 (2010).

19. W. R. Schwan, Regulation of fim genes in uropathogenic Escherichia coli, *World J. Clin. Infect. Dis.* **1**, 17–25 (2011).

20. G. D. Ehrlich, C. R. Arciola, From Koch's postulates to biofilm theory. The lesson of Bill Costerton, *Int. J. Artif. Organs* **35**, 695–699 (2012).

21. C. A. Czaja, D. Scholes, T. M. Hooton, W. E. Stamm, Population-Based Epidemiologic Analysis of Acute Pyelonephritis, *Clin. Infect. Dis.* **45**, 273–280 (2007).

22. S. Yamamoto, T. Tsukamoto, A. Terai, H. Kurazono, Y. Takeda, Genetic evidence supporting the fecal-perineal-urethral hypothesis in cystitis caused by Escherichia coli, *J. Urol.* **157**, 1127–1129 (1997).

23. M. Grabe, in *Urologi*, J.-E. Damber, R. Peeker, Eds. (Studentlitteratur AB, Lund, 2012), pp. 397–416.

24. F. X. Choong, H. Antypas, A. Richter-Dahlfors, Integrated pathophysiology of pyelonephritis, *Microbiol. Spectr.* **3** (2015), doi:10.1128/microbiolspec.UTI-0014-2012.

25. K. G. Naber, W. Weidner, F. M. E. Wagenlehner, A. Pilatz, Urosepsis: Overview of the Diagnostic and Treatment Challenges, *Microbiol. Spectr.* **3** (2015), doi:10.1128/microbiolspec.UTI-0003-2012.

26. D. R. Hickling T. Sun and X. Wu, Anatomy and Physiology of the Urinary Tract: Relation to Host Defense and Microbial Infection, *Microbiol. Spectr.* **3**, (2016), doi:10.1128/microbiolspec.UTI-0016-2012

27. D. Eaton, J. Pooler, A. Vander, *Vander's Renal Physiology* (McGraw-Hill Medical, New York, NY, ed. 7th, 2009).

28. P. Chahales, D. G. Thanassi, Structure, Function,

and Assembly of Adhesive Organelles by Uropathogenic Bacteria, *Microbiol. Spectr.* **3** (2015), doi:10.1128/microbiolspec.UTI-0018-2013.

29. B. Wullt, G. Bergsten, M. Samuelsson, C. Svanborg, The role of P fimbriae for *Escherichia coli* establishment and mucosal inflammation in the human urinary tract, *Int. J. Antimicrob. Agents* **19**, 522–538 (2002).

30. M. Soderhall, U. Bergerheim, S. H. Jacobson, J. Lundahl, R. Möllby, S. Normark, J. Winberg, Molecular evidence for pap-G specific adhesion of Escherichia coli to human renal cells, *J. Urol.* **157**, 346–350 (1997).

31. G. Källenius, R. Möllby, H. Hultberg, S. B. Svenson, B. Cedergren, J. A. N. Winberg, Structure of carbohydrate part of receptor on human uroepithelial cells for pyelonephritogenic Escherichia coli, *Lancet* **318**, 604–606 (1981).

32. K. W. Dodson, J. S. Pinkner, T. Rose, G. Magnusson, S. J. Hultgren, G. Waksman, Structural basis of the interaction of the pyelonephritic E. coli adhesin to its human kidney receptor, *Cell* **105**, 733–743 (2001).

33. K. Bock, M. E. Breimer, A. Brignole, G. C. Hansson, K. A. Karlsson, G. Larson, H. Leffler, B. E. Samuelsson, N. Stromberg, C. S. Eden, et al., Specificity of binding of a strain of uropathogenic Escherichia coli to Gal alpha 1-4Gal-containing glycosphingolipids, *J Biol Chem* **260**, 8545–8551 (1985).

34. I. Johanson, K. Plos, B.-I. Marklund, C. Svanborg, Pap, papG and prsG DNA sequences in Escherichia coli from the fecal flora and the urinary tract, *Microb. Pathog.* **15**, 121–129 (1993).

35. N. Strömberg, B. I. Marklund, B. Lund, D. Ilver, a Hamers, W. Gaastra, K. a Karlsson, S. Normark, Host-specificity of uropathogenic Escherichia coli depends on differences in binding specificity to Gal alpha 1-4Gal-containing isoreceptors., *EMBO J.* **9**, 2001–2010 (1990).

36. M. C. Lane, H. L. T. Mobley, Role of P-fimbrial-mediated adherence in pyelonephritis and persistence of uropathogenic Escherichia coli (UPEC) in the mammalian kidney, *Kidney Int.* **72**, 19–25 (2007).

37. L. Hagberg, R. Hull, S. Hull, S. Falkow, R. Freter, C. Svanborg Edén, Contribution of adhesion to bacterial persistence in the mouse urinary tract, *Infect. Immun.* **40**, 265–272 (1983).

38. H. L. T. Mobley, K. G. Jarvis, J. P. Elwood, D. I. Whittle, C. V. Lockatell, R. G. Russell, D. E. Johnson, M. S. Donnenberg, J. W. Warren, Isogenic P-fimbrial deletion mutants of pyelonephritogenic Escherichia coli: the role of α Gal(1–4)β Gal binding in virulence of a wild‐type strain, *Mol. Microbiol.* **10**, 143–155 (1993).

39. J. A. Roberts, B. I. Marklund, D. Ilver, D. Haslam, M. B. Kaack, G. Baskin, M. Louis, R. Möllby, J. Winberg, S. Normark, The Gal(alpha 1-4)Gal-specific tip adhesin of Escherichia coli P-fimbriae is needed for pyelonephritis to occur in the normal urinary tract, *Proc. Natl. Acad. Sci. U. S. A.* **91**, 11889–11893 (1994).

40. B. Lanne, B. M. Olsson, P. A. Jovall, J. Angstrom, H. Linder, B. I. Marklund, J. Bergstrom, K. A. Karlsson, Glycoconjugate receptors for P-fimbriated Escherichia coli in the mouse*J. Biol. Chem.* **270**, 9017–9025 (1995).

41. L. E. Månsson, K. Melican, J. Boekel, R. M. Sandoval, I. Hautefort, G. A. Tanner, B. A. Molitoris, A. Richter-Dahlfors, Real-time studies of the progression of bacterial infections and immediate tissue responses in live animals, *Cell. Microbiol.* **9**, 413–424 (2007).

42. K. Melican, R. M. Sandoval, A. Kader, L. Josefsson, G. A. Tanner, B. A. Molitoris, A. Richter-Dahlfors, Uropathogenic Escherichia coli P and Type 1 fimbriae act in synergy in a living host to facilitate renal colonization leading to nephron obstruction, *PLoS Pathog.* **7**, e1001298 (2011).

43. M. Rahdar, A. Rashki, H. R. Miri, M. R. Ghalehnoo, Detection of pap, sfa, afa, foc, and fim adhesin-encoding operons in uropathogenic Escherichia coli isolates collected from patients with urinary tract infection, *Jundishapur J. Microbiol.* **8**, e22647 (2015).

44. M. Arthur, C. E. Johnson, R. H. Rubin, R. D. Arbeit, C. Campanelli, C. Kim, S. Steinbach, M. Agarwal, R. Wilkinson, R. Goldstein, Molecular epidemiology of adhesin and hemolysin virulence factors among uropathogenic Escherichia coli, *Infect. Immun.* **57**, 303–313 (1989).

45. G. Zhou, W.-J. Mo, P. Sebbel, G. Min, T. A. Neubert, R. Glockshuber, X.-R. Wu, T.-T. Sun, X.-P. Kong, Uroplakin Ia is the urothelial receptor for uropathogenic *Escherichia coli*: evidence from in vitro FimH binding, *J. Cell Sci.* **114**, 4095–4103 (2001).

46. B. Xie, G. Zhou, S.-Y. Chan, E. Shapiro, X.-P. Kong, X.-R. Wu, T.-T. Sun, C. E. Costello, Distinct glycan structures of uroplakins Ia and Ib: structural basis for the selective binding of FimH adhesin to uroplakin Ia, *J. Biol. Chem.* **281**, 14644–14653 (2006).

47. X. R. Wu, J. H. Lin, T. Walz, M. Haner, J. Yu, U. Aebi, T. T. Sun, Mammalian uroplakins. A group of highly conserved urothelial differentiation-related membrane proteins, *J. Biol. Chem.* **269**, 13716–13724 (1994).

48. R. Stenutz, A. Weintraub, G. Widmalm, The structures of Escherichia coli O-polysaccharide antigens, *FEMS Microbiol. Rev.* **30**, 382–403 (2006).

49. H. C. Flemming, J. Wingender, The biofilm matrix*Nat. Rev. Microbiol.* **8**, 623–633 (2010).

50. H. C. Flemming, J. Wingender, U. Szewzyk, P.

Steinberg, S. A. Rice, S. Kjelleberg, Biofilms: An emergent form of bacterial life, *Nat. Rev. Microbiol.* **14**, 563–575 (2016).

51. N. Høiby, T. Bjarnsholt, C. Moser, G. L. Bassi, T. Coenye, G. Donelli, L. Hall-Stoodley, V. Holá, C. Imbert, K. Kirketerp-Møller, D. Lebeaux, A. Oliver, A. J. Ullmann, C. Williams, ESCMID Study Group for Biofilms (ESGB), Consulting External Expert Werner Zimmerli, ESCMID* guideline for the diagnosis and treatment of biofilm infections 2014, *Clin. Microbiol. Infect.* **21**, S1–S25 (2015).

52. O. Ciofu, E. Rojo-Molinero, M. D. Macia, A. Oliver, Antibiotic treatment of biofilm infections, *APMIS* **125**, 304–319 (2017).

53. M. C. Walters III, F. Roe, A. Bugnicourt, M. J. Franklin, P. S. Stewart, Contributions of Antibiotic Penetration, Oxygen Limitation, and Low Metabolic Activity to Tolerance of Pseudomonas aeruginosa Biofilms to Ciprofloxacin and Tobramycin, *Antimicrob. Agents Chemother.* **47**, 317–323 (2003).

54. W. C. Chiang, M. Nilsson, P. Ø. Jensen, N. Høiby, T. E. Nielsen, M. Givskov, T. Tolker-Nielsen, Extracellular DNA shields against aminoglycosides in Pseudomonas aeruginosa biofilms, *Antimicrob. Agents Chemother.* **57**, 2352–2361 (2013).

55. H. Mulcahy, L. Charron-Mazenod, S. Lewenza, Extracellular DNA chelates cations and induces antibiotic resistance in Pseudomonas aeruginosa biofilms, *PLoS Pathog.* **4**, e1000213 (2008).

56. N. Bagge, M. Hentzer, J. B. Andersen, O. Ciofu, M. Givskov, N. Høiby, Dynamics and spatial distribution of beta-lactamase expression in Pseudomonas aeruginosa biofilms., *Antimicrob. Agents Chemother.* **48**, 1168–1174 (2004).

57. A. Brooun, S. H. Liu, K. Lewis, A dose-response study of antibiotic resistance in Pseudomonas aeruginosa biofilms, *Antimicrob. Agents Chemother.* **44**, 640–646 (2000).

58. K. Lewis, Persister Cells, *Annu. Rev. Microbiol.* **64**, 357–372 (2010).

59. K. N. Kragh, M. Alhede, P. Jensen, C. Moser, T. Scheike, C. S. Jacobsen, S. S. Poulsen, S. R. Eickhardt-Sørensen, H. Trøstrup, L. Christoffersen, H. P. Hougen, L. F. Rickelt, M. Kühl, N. Høiby, T. Bjarnsholt, Polymorphonuclear leukocytes restrict growth of Pseudomonas aeruginosa in the lungs of cystic fibrosis patients, *Infect. Immun.* **82**, 4477–4486 (2014).

60. M. R. Parsek, P. K. Singh, Bacterial biofilms: an emerging link to disease pathogenesis, *Annu.Rev.Microbiol.* **57**, 677–701 (2003).

61. H. S. Choe, S. W. Son, H. A. Choi, H. J. Kim, S. G. Ahn, J. H. Bang, S. J. Lee, J. Y. Lee, Y. H. Cho, S. S. Lee, Analysis of the distribution of bacteria within urinary catheter biofilms using four different molecular techniques, *Am. J. Infect. Control* **40**, E249–E254 (2012).

62. D. N. Frank, S. S. Wilson, A. L. St. Amand, N. R. Pace, Culture-independent microbiological analysis of Foley urinary catheter biofilms, *PLoS One* **4**, e7811 (2009).

63. Y. Xu, C. Moser, W. A. Al-Soud, S. Sørensen, N. Høiby, P. H. Nielsen, T. R. Thomsen, Culture-dependent and -independent investigations of microbial diversity on urinary catheters, *J. Clin. Microbiol.* **50**, 3901–3908 (2012).

64. T. Bjarnsholt, P. Ø. Jensen, M. J. Fiandaca, J. Pedersen, C. R. Hansen, C. B. Andersen, T. Pressler, M. Givskov, N. Høiby, Pseudomonas aeruginosa biofilms in the respiratory tract of cystic fibrosis patients, *Pediatr. Pulmonol.* **44**, 547–558 (2009).

65. S. Malic, K. E. Hill, A. Hayes, S. L. Percival, D. W. Thomas, D. W. Williams, Detection and identification of specific bacteria in wound biofilms using peptide nucleic acid fluorescent in situ hybridization (PNA FISH), *Microbiology* **155**, 2603–2611 (2009).

66. N. Hoffmann, T. B. T. Rasmussen, P. P. Jensen, C. Stub, M. Hentzer, S. Molin, O. Ciofu, M. Givskov, H. K. Johansen, N. Høiby, Novel mouse model of chronic Pseudomonas aeruginosa lung infection mimicking cystic fibrosis, *Infect. Immun.* **73**, 2504–2514 (2005).

67. L. Yang, J. A. J. Haagensen, L. Jelsbak, H. K. Johansen, C. Sternberg, N. Høiby, S. Molin, In situ growth rates and biofilm development of Pseudomonas aeruginosa populations in chronic lung infections, *J. Bacteriol.* **190**, 2767–2776 (2008).

68. T. R. Neu, G. D. W. Swerhone, J. R. Lawrence, Assessment of lectin- binding analysis for in situ detection of glycoconjugates in biofilm systems, *Microbiology* **147**, 299–313 (2001).

69. A. R. Johnsen, M. Hausner, A. Schnell, S. Wuertz, Evaluation of fluorescently labeled lectins for noninvasive localization of extracellular polymeric substances in Sphingomonas biofilms, *Appl. Environ. Microbiol.* **66**, 3487–3491 (2000).

70. Y. Kai-Larsen, P. Lüthje, M. Chromek, V. Peters, X. Wang, Å. Holm, L. Kádas, K. O. Hedlund, J. Johansson, M. R. Chapman, S. H. Jacobson, U. Römling, B. Agerberth, A. Brauner, Uropathogenic Escherichia coli modulates immune responses and its curli fimbriae interact with the antimicrobial peptide LL-37, *PLoS Pathog.* **6**, e1001010 (2010).

71. A. Åslund, K. P. R. Nilsson, P. Konradsson, Fluorescent oligo and poly-thiophenes and their utilization for recording biological events of diverse origin-when organic chemistry meets biology, *J. Chem. Biol.* **2**, 161–175 (2009).

72. T. Klingstedt, H. Shirani, K. O. A. Åslund, N. J. Cairns, C. J. Sigurdson, M. Goedert, K. P. R. Nilsson, The structural basis for optimal performance of oligothiophene-based fluorescent amyloid ligands:

Conformational flexibility is essential for spectral assignment of a diversity of protein aggregates, *Chem. Eur. J.* **19**, 10179–10192 (2013).

73. D. Sjölander, thesis, Linköping University (2014).

74. F. X. Choong, M. Bäck, S. Fahlén, L. B. G. Johansson, K. Melican, M. Rhen, K. P. R. Nilsson, A. Richter-Dahlfors, Real-time optotracing of curli and cellulose in live Salmonella biofilms using luminescent oligothiophenes, *Npj Biofilms Microbiomes* **2**, 16024 (2016).

75. F. X. Choong, M. Bäck, A. Schulz, K. P. R. Nilsson, U. Edlund, A. Richter-Dahlfors, Stereochemical identification of glucans by oligothiophenes enables cellulose anatomical mapping in plant tissues, *Sci. Rep.* **8**, 3108 (2018).

76. X. Zogaj, M. Nimtz, M. Rohde, W. Bokranz, U. Römling, The multicellular morphotypes of Salmonella typhimurium and Escherichia coli produce cellulose as the second component of the extracellular matrix, *Mol. Microbiol.* **39**, 1452–1463 (2001).

77. B. Foxman, Recurring urinary tract infection: Incidence and risk factors, *Am. J. Public Health* **80**, 331–333 (1990).

78. M. Glover, C. G. Moreira, V. Sperandio, P. Zimmern, Recurrent urinary tract infections in healthy and nonpregnant women, *Urol. Sci.* **25**, 1–8 (2014).

79. S. M. Soto, A. Smithson, J. P. Horcajada, J. A. Martinez, J. P. Mensa, J. Vila, Implication of biofilm formation in the persistence of urinary tract infection caused by uropathogenic Escherichia coli, *Clin. Microbiol. Infect.* **12**, 1034–1036 (2006).

80. J. C. Nickel, J. W. Costerton, Bacterial localization in antibiotic-refractory chronic bacterial prostatitis, *Prostate* **23**, 107–114 (1993).

81. S. S. Justice, C. Hung, J. A. Theriot, D. A. Fletcher, G. G. Anderson, M. J. Footer, S. J. Hultgren, Differentiation and developmental pathways of uropathogenic *Escherichia coli* in urinary tract pathogenesis, *Proc. Natl. Acad. Sci. U. S. A.* **101**, 1333–1338 (2004).

82. L. Robino, P. Scavone, L. Araujo, G. Algorta, P. Zunino, M. C. Pírez, R. Vignoli, Intracellular bacteria in the pathogenesis of Escherichia coli urinary tract infection in children, *Clin. Infect. Dis.* **59**, e158–e164 (2014).

83. D. A. Rosen, T. M. Hooton, W. E. Stamm, P. A. Humphrey, S. J. Hultgren, Detection of intracellular bacterial communities in human urinary tract infection, *PLoS Med.* **4**, e329 (2007).

84. C. L. Ventola, The antibiotic resistance crisis: part 1: causes and threats, *P T* **40**, 277–283 (2015).

85. R. Cantón, M. I. Morosini, Emergence and spread of antibiotic resistance following exposure to antibiotics, *FEMS Microbiol. Rev.* **35**, 977–991 (2011).

86. World Health Organization, *Global action plan on antimicrobial resistance* (Geneva, 2015; http://www.who.int/drugresistance/global_action_plan/en/).

87. M. Davenport, K. E. Mach, L. M. D. Shortliffe, N. Banaei, T. H. Wang, J. C. Liao, New and developing diagnostic technologies for urinary tract infections, *Nat. Rev. Urol.* **14**, 298–310 (2017).

88. P. Pietrucha-Dilanchian, T. M. Hooton, Diagnosis, Treatment, and Prevention of Urinary Tract Infection, *Microbiol. Spectr.* **4**, UTI-0021-2015 (2015).

89. M. L. Wilson, L. Gaido, Laboratory diagnosis of urinary tract infections in adult patients, *Med. Microbiol.* **38**, 1150–1158 (2004).

90. E. Yusuf, B. Van Herendael, J. Van Schaeren, Performance of urinalysis tests and their ability in predicting results of urine cultures: A comparison between automated test strip analyser and flow cytometry in various subpopulations and types of samples, *J. Clin. Pathol.* **70**, 631–636 (2017).

91. H. A. D'Souza, M. Campbell, E. J. Baron, Practical Bench Comparison of BBL CHROMagar Orientation and Standard Two-Plate Media for Urine Cultures, *J. Clin. Microbiol.* **42**, 60–64 (2004).

92. J. H. Jorgensen, M. J. Ferraro, Antimicrobial Susceptibility Testing: A Review of General Principles and Contemporary Practices, *Clin. Infect. Dis.* **49**, 1749–1755 (2009).

93. R. Schwalbe, L. Steele-Moore, A. C. Goodwin, Eds., *Antimicrobial Susceptibility Testing Protocols* (CRC Press, Boca Raton, FL, 2007).

94. The European Committee on Antimicrobial Susceptibility Testing, Direct antimicrobial susceptibility testing guidelines (2012).

95. J. Avesar, D. Rosenfeld, M. Truman-Rosentsvit, T. Ben-Arye, Y. Geffen, M. Bercovici, S. Levenberg, Rapid phenotypic antimicrobial susceptibility testing using nanoliter arrays, *Proc. Natl. Acad. Sci. U. S. A.* **114**, E5787–E5795 (2017).

96. M. Sundqvist, J. Olafsson, E. Matuschek, EUCAST breakpoints can be used to interpret direct susceptibility testing of Enterobacteriaceae from urine samples, *APMIS* **123**, 152–155 (2015).

97. A. Mezger, E. Gullberg, J. Göransson, A. Zorzet, D. Herthnek, E. Tano, M. Nilsson, D. I. Andersson, A general method for rapid determination of antibiotic susceptibility and species in bacterial infections, *J. Clin. Microbiol.* **53**, 425–432 (2015).

98. N. G. Schoepp, T. S. Schlappi, M. S. Curtis, S. S. Butkovich, S. Miller, R. M. Humphries, R. Ismagilov, Pathogen-specific Phenotypic Antibiotic Susceptibility Test Directly from Clinical Samples in as Fast as 30 Minutes Using Digital LAMP

Quantification, *Sci. Transl. Med.* **9**, eaal3693 (2017).

99. A. Pantel, J. Monier, J.-P. Lavigne, Performance of the Accelerate Pheno™ system for identification and antimicrobial susceptibility testing of a panel of multidrug-resistant Gram-negative bacilli directly from positive blood cultures, *J. Antimicrob. Chemother.* **73**, 1546–1552 (2018).

100. P. Pancholi, K. C. Carroll, B. W. Buchan, R. C. Chan, N. Dhiman, B. Ford, P. A. Granato, A. T. Harrington, D. R. Hernandez, R. M. Humphries, M. R. Jindra, N. A. Ledeboer, S. A. Miller, A. Brian Mochon, M. A. Morgan, R. Patel, P. C. Schreckenberger, P. D. Stamper, P. J. Simner, N. E. Tucci, C. Zimmerman, D. M. Wolk, Multicenter evaluation of the accelerate PhenoTest BC kit for rapid identification and phenotypic antimicrobial susceptibility testing using morphokinetic cellular analysis, *J. Clin. Microbiol.* **56**, e01329-17 (2018).

101. S. W. Metzger, D. C. Howson, D. A. Goldberg, D. A. Buttry, Rapid microbial detection and antimicrobial susceptibility testing (2008), US Patent No 7,341,841 B2.

102. A. W. Bauer, W. M. Kirby, J. C. Sherris, M. Turck, Antibiotic susceptibility testing by a standardized single disk method, *Am. J. Clin. Pathol.* **45**, 493–496 (1966).

103. J. H. Jorgensen, J. D. Turnidge, in *Manual of clinical microbiology*, (American Society for Microbiology (Blackwell Publishing), 2007), pp. 1152–1172.

104. Clinical and Laboratory Standards Institute, *Methods for Dilution Antimicrobial Susceptibility Tests for Bacteria That Grow Aerobically. Approved Standard M7-A10* (Clinical and Laboratory Standards Institute, Wayne, PA, ed. 9, 2012).

105. G. B. Williams, D. M. Nothaft, G. F. Enscoe, K. N. Burtner, M. E. Kangas, Combined rapid susceptibility assay and microorganism identification system (2005), European Patent No EP1177448A2.

106. R. C. Fader, E. Weaver, R. Fossett, M. Toyras, J. Vanderlaan, D. Gibbs, A. Wang, N. Thierjung, Multilaboratory study of the biomic automated well-reading instrument versus microscan walkaway for reading microscan antimicrobial susceptibility and identification panels, *J. Clin. Microbiol.* **51**, 1548–1554 (2013).

107. J. W. Snyder, G. K. Munier, C. L. Johnson, Direct comparison of the BD phoenix system with the MicroScan WalkAway system for identification and antimicrobial susceptibility testing of Enterobacteriaceae and nonfermentative gram-negative organisms, *J. Clin. Microbiol.* **46**, 2327–2333 (2008).

108. P. Sellenriek, J. Holmes, R. Ferrett, R. Drury, G. A. Storch, in *105th General Meeting of the American Society for Microbiology*, (American Society for Microbiology, Washington, DC, 2005).

109. S. A. Mittman, R. C. Huard, P. Della-Latta, S. Whittier, Comparison of BD Phoenix to Vitek 2, MicroScan MICroSTREP, and Etest for antimicrobial susceptibility testing of Streptococcus pneumoniae, *J. Clin. Microbiol.* **47**, 3557–3561 (2009).

110. R. E. O'Bear, B. Colin, G. R. Tegeler, J. L. Staples, Sample Card (1997), US Patent No 5,609,828.

111. FDA, 510(k) Substantial equivalence determination decision summary Number: K151320 (2013).

112. F. Garcia-Garrote, E. Cercenado, E. Bouza, Evaluation of a new system, VITEK 2, for identification and antimicrobial susceptibility testing of enterococci, *J. Clin. Microbiol.* **38**, 2108–2111 (2000).

113. M. Marschal, J. Bachmaier, I. Autenrieth, P. Oberhettinger, M. Willmann, S. Peter, Evaluation of the Accelerate Pheno system for fast identification and antimicrobial susceptibility testing from positive blood cultures in bloodstream infections caused by Gram-negative pathogens, *J. Clin. Microbiol.* **55**, 2116–2126 (2017).

114. V. Perreten, L. Vorlet-fawer, P. Slickers, R. Ehricht, P. Kuhnert, J. Frey, Microarray-Based Detection of 90 Antibiotic Resistance Genes of Gram-Positive Bacteria, *J Clin Microbiol* **43**, 2291–2302 (2005).

115. A. Sinclair, C. Arnold, N. Woodford, Rapid Detection and Estimation by Pyrosequencing of 23S rRNA Genes with a Single Nucleotide Polymorphism Conferring Linezolid Resistance in Enterococci, *Antimicrob. Agents Chemother.* **47**, 3620–3622 (2003).

116. R. Rossau, H. Traore, H. De Beenhouwer, W. Mijs, G. Jannes, P. De Rijk, F. Portaels, Evaluation of the INNO-LiPA Rif . TB assay , a reverse hybridization assay for the simultaneous detection of Mycobacterium tuberculosis complex and its resistance to rifampicin, *Antimicrob. Agents Chemother.* **41**, 2093–2098 (1997).

117. A. S. Rossney, C. M. Herra, M. M. Fitzgibbon, P. M. Morgan, M. J. Lawrence, B. O'Connell, Evaluation of the IDI-MRSA assay on the SmartCycler real-time PCR platform for rapid detection of MRSA from screening specimens, *Eur. J. Clin. Microbiol. Infect. Dis.* **26**, 459–466 (2007).

118. N. Woodford, A. Sundsfjord, Molecular detection of antibiotic resistance: When and where?, *J. Antimicrob. Chemother.* **56**, 259–261 (2005).

119. J. Volman, M. L. Gray, M. A. Schmidt, Microfabrication in biology and medicine, *Annu. Rev. Biomed. Eng.* **01**, 401–425 (1999).

120. S. N. Bhatia, D. E. Ingber, Microfluidic organs-on-chips, *Nat. Biotechnol.* **32**, 760–772 (2014).

121. D. B. Weibel, W. R. DiLuzio, G. M.

Whitesides, Microfabrication meets microbiology, *Nat. Rev. Microbiol.* **5**, 209–218 (2007).

122. S. Lindström, H. Andersson-Svahn, Miniaturization of biological assays - Overview on microwell devices for single-cell analyses, *Biochim. Biophys. Acta* **1810**, 308–316 (2011).

123. A. E. Barber, J. P. Norton, T. J. Wiles, M. A. Mulvey, Strengths and Limitations of Model Systems for the Study of Urinary Tract Infections and Related Pathologies, **80**, 351–367 (2016).

124. P. Uhlen, A. Laestadius, T. Jahnukainen, T. Soderblom, F. Backhed, G. Celsi, H. Brismar, S. Normark, A. Aperia, A. Richter-Dahlfors, α-Haemolysin of uropathogenic E.coli induces Ca2+ oscillations in renal epithelial cells, *Nature* **405**, 694–697 (2000).

125. F. Bäckhed, M. Söderhäll, P. Ekman, S. Normark, A. Richter-Dahlfors, Induction of innate immune responses by Escherichia coli and purified lipopolysaccharide correlate with organ- and cell-specific expression of Toll-like receptors within the human urinary tract, *Cell. Microbiol.* **3**, 153–158 (2001).

126. F. Bäckhed, B. Alsén, N. Roche, J. Ångström, A. Von Euler, M. E. Breimer, B. Westerlund-Wikström, S. Teneberg, A. Richter-Dahlfors, Identification of target tissue glycosphingolipid receptors for uropathogenic, F1C-fimbriated Escherichia coli and its role in mucosal inflammation, *J. Biol. Chem.* **277**, 18198–18205 (2002).

127. K. Li, W. Zhou, Y. Hong, S. H. Sacks, N. S. Sheerin, Synergy between type 1 fimbriae expression and C3 opsonisation increases internalisation of E. coli by human tubular epithelial cells, *BMC Microbiol.* **9** (2009), doi:10.1186/1471-2180-9-64.

128. D. M. Guyer, S. Radulovic, F. E. Jones, H. L. T. Mobley, Sat, the secreted autotransporter toxin of uropathogenic Escherichia coli, is a vacuolating cytotoxin for bladder and kidney epithelial cells, *Infect. Immun.* **70**, 4539–4546 (2002).

129. M. Essig, G. Friedlander, Tubular shear stress and phenotype of renal proximal tubular cells, *J. Am. Soc. Nephrol.* **14**, S33–S35 (2003).

130. Y. Duan, N. Gotoh, Q. Yan, Z. Du, A. M. Weinstein, T. Wang, S. Weinbaum, Shear-induced reorganization of renal proximal tubule cell actin cytoskeleton and apical junctional complexes, *Proc. Natl. Acad. Sci. U. S. A.* **105**, 11418–11423 (2008).

131. E. V. Sokurenko, V. Vogel, W. E. Thomas, Catch-Bond Mechanism of Force-Enhanced Adhesion: Counterintuitive, Elusive, but ... Widespread?, *Cell Host Microbe* **4**, 314–323 (2008).

132. I. Le Trong, P. Aprikian, B. A. Kidd, M. Forero-Shelton, V. Tchesnokova, P. Rajagopal, V. Rodriguez, G. Interlandi, R. Klevit, V. Vogel, R. E. Stenkamp, E. V. Sokurenko, W. E. Thomas, Structural Basis for Mechanical Force Regulation of the Adhesin FimH via Finger Trap-like β Sheet Twisting, *Cell* **141**, 645–655 (2010).

133. W. E. Thomas, E. Trintchina, M. Forero, V. Vogel, E. V. Sokurenko, Bacterial adhesion to target cells enhanced by shear force, *Cell* **109**, 913–923 (2002).

134. W. E. Thomas, L. M. Nilsson, M. Forero, E. V. Sokurenko, V. Vogel, Shear-dependent "stick-and-roll" adhesion of type 1 fimbriated Escherichia coli, *Mol. Microbiol.* **53**, 1545–1557 (2004).

135. D. E. Ingber, Reverse Engineering Human Pathophysiology with Organs-on-Chips, *Cell* **164**, 1105–1109 (2016).

136. Y.-C. Toh, T. C. Lim, D. Tai, G. Xiao, D. van Noort, H. Yu, A microfluidic 3D hepatocyte chip for drug toxicity testing, *Lab Chip* **9**, 2026–2035 (2009).

137. A. Sivaraman, J. K. Leach, S. Townsend, T. Iida, B. J. Hogan, D. B. Stolz, R. Fry, S. R. Tannenbaum, L. G. Griffith, A Microscale In Vitro Physiological Model of the Liver : Predictive Screens for Drug Metabolism and Enzyme Induction, *Curr. Drug Metab.* **6**, 569–591 (2005).

138. E. Novik, T. J. Maguire, P. Chao, K. C. Cheng, M. L. Yarmush, A microfluidic hepatic coculture platform for cell-based drug metabolism studies, *Biochem. Pharmacol.* **79**, 1036–1044 (2010).

139. P. Chao, T. Maguire, E. Novik, K.-C. Cheng, M. L. Yarmush, Evaluation of a microfluidic based cell culture platform with primary human hepatocytes for the prediction of hepatic clearance in human, *Biochem. Pharmacol.* **78**, 625–32 (2009).

140. A. Carraro, W.-M. Hsu, K. M. Kulig, W. S. Cheung, M. L. Miller, E. J. Weinberg, E. F. Swart, M. Kaazempur-Mofrad, J. T. Borenstein, J. P. Vacanti, C. Neville, In vitro analysis of a hepatic device with intrinsic microvascular-based channels, *Biomed. Microdevices* **10**, 795–805 (2008).

141. R. Baudoin, L. Griscom, M. Monge, C. Legallais, E. Leclerc, Development of a renal microchip for in vitro distal tubule models, *Biotechnol. Prog.* **23**, 1245–1253 (2007).

142. E. M. Frohlich, X. Zhang, J. L. Charest, The use of controlled surface topography and flow-induced shear stress to influence renal epithelial cell function, *Integr. Biol.* **4**, 75–83 (2012).

143. K.-J. Jang, A. P. Mehr, G. A. Hamilton, L. A. McPartlin, S. Chung, K.-Y. Suh, D. E. Ingber, Human kidney proximal tubule-on-a-chip for drug transport and nephrotoxicity assessment, *Integr. Biol.* **5**, 1119–1129 (2013).

144. K.-J. Jang, K.-Y. Suh, A multi-layer microfluidic device for efficient culture and analysis of renal tubular cells, *Lab Chip* **10**, 36–42 (2010).

145. L. C. Snouber, F. Letourneur, P. Chafey, C. Broussard, M. Monge, C. Legallais, E. Leclerc,

Analysis of transcriptomic and proteomic profiles demonstrates improved Madin-Darby canine kidney cell function in a renal microfluidic biochip, *Biotechnol. Prog.* **28**, 474–484 (2011).

146. D. Huh, D. C. Leslie, B. D. Matthews, J. P. Fraser, S. Jurek, G. A. Hamilton, K. S. Thorneloe, M. A. Mcalexander, D. E. Ingber, A Human Disease Model of Drug Toxicity-Induced Pulmonary Edema in a Lung-on-a-Chip Microdevice, *Sci. Transl. Med.* **4**, 159ra147 (2012).

147. D. Huh, B. D. Matthews, A. Mammoto, M. Montoya-Zavala, H. Y. Hsin, D. E. Ingber, Reconstituting organ-level lung functions on a chip, *Science* **328**, 1662–1668 (2010).

148. H. J. Kim, D. Huh, G. Hamilton, D. E. Ingber, Human gut-on-a-chip inhabited by microbial flora that experiences intestinal peristalsis-like motions and flow, *Lab Chip* **12**, 2165–2174 (2012).

149. H. J. Kim, D. E. Ingber, Gut-on-a-Chip microenvironment induces human intestinal cells to undergo villus differentiation, *Integr. Biol.* **5**, 1130–1140 (2013).

150. B. M. Maoz, A. Herland, O. Y. F. Henry, W. D. Leineweber, M. Yadid, J. Doyle, R. Mannix, V. J. Kujala, E. A. Fitzgerald, K. K. Parker, D. E. Ingber, Organs-on-Chips with combined multi-electrode array and transepithelial electrical resistance measurement capabilities, *Lab Chip* **17**, 2294–2302 (2017).

151. A. Herland, A. D. Van Der Meer, E. A. FitzGerald, T. E. Park, J. J. F. Sleeboom, D. E. Ingber, Distinct contributions of astrocytes and pericytes to neuroinflammation identified in a 3D human blood-brain barrier on a chip, *PLoS One* **11**, e0150360 (2016).

152. E. Mairey, A. Genovesio, E. Donnadieu, C. Bernard, F. Jaubert, E. Pinard, J. Seylaz, J.-C. Olivo-Marin, X. Nassif, G. Duménil, Cerebral microcirculation shear stress levels determine Neisseria meningitidis attachment sites along the blood-brain barrier, *J. Exp. Med.* **203**, 1939–1950 (2006).

153. G. Mikaty, M. Soyer, E. Mairey, N. Henry, D. Dyer, K. T. Forest, P. Morand, S. Guadagnini, M. C. Prévost, X. Nassif, G. Duménil, Extracellular bacterial pathogen induces host cell surface reorganization to resist shear stress, *PLoS Pathog.* **5**, e1000314 (2009).

154. J. Claes, L. Liesenborghs, M. Lox, P. Verhamme, T. Vanassche, M. Peetermans, In Vitro and In Vivo Model to Study Bacterial Adhesion to the Vessel Wall Under Flow Conditions, *J. Vis. Exp.* **100**, e52862 (2015).

155. T. E. Andersen, S. Khandige, M. Madelung, J. Brewer, H. J. Kolmos, J. Møller-Jensen, Escherichia coli uropathogenesis In vitro: Invasion, cellular escape, and secondary infection analyzed in a human bladder cell infection model, *Infect. Immun.* **80**, 1858–1867 (2012).

156. M. Y. Galperin, E. V. Koonin, From complete genome sequence to "complete" understanding?, *Trends Biotechnol.* **28**, 398–406 (2010).

157. P. D. Karp, I. M. Keseler, A. Shearer, M. Latendresse, M. Krummenacker, S. M. Paley, I. Paulsen, J. Collado-Vides, S. Gama-Castro, M. Peralta-Gil, A. Santos-Zavaleta, M. I. Peñaloza-Spínola, C. Bonavides-martinez, J. Ingraham, Multidimensional annotation of the Escherichia coli K-12 genome, *Nucleic Acids Res.* **35**, 7577–7590 (2007).

158. R. J. Petri, A minor modification of the plating technique of Koch, *Cent. für bacterriologie und Parasittenkd.* **1**, 279–280 (1887).

159. W. Hesse, Walther and Angelina Hesse-Early Contributors to Bacteriology, *ASM News* **58**, 425–428 (1992).

160. R. Martinez, U. Schwaneberg, A roadmap to directed enzyme evolution and screening systems for biotechnological applications, *Biol. Res.* **46**, 395–405 (2013).

161. A. Blomberg, Measuring growth rate in high-throughput growth phenotyping, *Curr. Opin. Biotechnol.* **22**, 94–102 (2011).

162. J. Warringer, E. Ericson, L. Fernandez, O. Nerman, A. Blomberg, High-resolution yeast phenomics resolves different physiological features in the saline response, *Proc. Natl. Acad. Sci.* **100**, 15724–15729 (2003).

163. J. Warringer, D. Anevski, B. Liu, A. Blomberg, Chemogenetic fingerprinting by analysis of cellular growth dynamics, *BMC Chem. Biol.* **8** (2008), doi:10.1186/1472-6769-8-3.

164. S. Lindström, H. Andersson-Svahn, Overview of single-cell analyses: microdevices and applications, *Lab Chip* **10**, 3363–3372 (2010).

165. D. Nichols, N. Cahoon, E. M. Trakhtenberg, L. Pham, A. Mehta, A. Belanger, T. Kanigan, K. Lewis, S. S. Epstein, Use of ichip for high-throughput in situ cultivation of "uncultivable microbial species, *Appl. Environ. Microbiol.* **76**, 2445–2450 (2010).

166. L. L. Ling, T. Schneider, A. J. Peoples, A. L. Spoering, I. Engels, B. P. Conlon, A. Mueller, T. F. Schäberle, D. E. Hughes, S. Epstein, M. Jones, L. Lazarides, V. A. Steadman, D. R. Cohen, C. R. Felix, K. A. Fetterman, W. P. Millett, A. G. Nitti, A. M. Zullo, C. Chen, K. Lewis, A new antibiotic kills pathogens without detectable resistance, *Nature* **517**, 455–459 (2015).

167. W. R. DiLuzio, L. Turner, M. Mayer, P. Garstecki, D. B. Weibel, H. C. Berg, G. M. Whitesides, Escherichia coli swim on the right-hand side, *Nature* **435**, 1271–1274 (2005).

168. H. Mao, P. S. Cremer, M. D. Manson, A sensitive, versatile microfluidic assay for bacterial

chemotaxis, *Proc. Natl. Acad. Sci.* **100**, 5449–5454 (2003).

169. F. K. Balagaddé, L. You, C. L. Hansen, F. H. Arnold, S. R. Quake, Long-Term Monitoring of Bacteria Undergoing Programmed Population Control in a Microchemostat, *Science* **309**, 137–140 (2005).

170. K. Nagamine, S. Onodera, Y. S. Torisawa, T. Yasukawa, H. Shiku, T. Matsue, On-chip transformation of bacteria, *Anal. Chem.* **77**, 4278–4281 (2005).

171. Y. Lu, J. Gao, D. D. Zhang, V. Gau, J. C. Liao, P. K. Wong, Single cell antimicrobial susceptibility testing by confined microchannels and electrokinetic loading, *Anal. Chem.* **85**, 3971–3976 (2013).

172. Ö. Baltekin, A. Boucharin, E. Tano, D. I. Andersson, J. Elf, Antibiotic susceptibility testing in less than 30 min using direct single-cell imaging, *Proc. Natl. Acad. Sci.* **114**, 9170–9175 (2017).

173. J. Choi, J. Yoo, M. Lee, E.-G. Kim, J. S. Lee, S. Lee, S. Joo, S. H. Song, E.-C. Kim, J. C. Lee, H. C. Kim, Y.-G. Jung, S. Kwon, A rapid antimicrobial susceptibility test based on single-cell morphological analysis, *Sci. Transl. Med.* **6**, 267ra174 (2014).

174. Z. Hou, Y. An, K. Hjort, K. Hjort, L. Sandegren, Z. Wu, Time lapse investigation of antibiotic susceptibility using a microfluidic linear gradient 3D culture device, *Lab Chip* **14**, 3409–3418 (2014).

175. Y. Matsumoto, S. Sakakihara, A. Grushnikov, K. Kikuchi, H. Noji, A. Yamaguchi, R. Iino, Y. Yagi, K. Nishino, A microfluidic channel method for rapid drug-susceptibility testing of Pseudomonas aeruginosa, *PLoS One* **11**, e0148797 (2016).

176. S. Lindström, R. Larsson, H. A. Svahn, Towards high-throughput single cell/clone cultivation and analysis, *Electrophoresis* **29**, 1219–1227 (2008).

177. S. Lindström, M. Eriksson, T. Vazin, J. Sandberg, J. Lundeberg, J. Frisén, H. Andersson-Svahn, High-density microwell chip for culture and analysis of stem cells, *PLoS One* **4**, e6997 (2009).

178. Clinical and Laboratory Standars Institute, *Performance standards for antimicrobial susceptibility testing; twenty-third informational supplement* (Clinical and Laboratory Standars Institute, Wayne, PA, 2013).

179. D. S. Burgess, R. G. Hall, In vitro killing of parenteral beta-lactams against standard and high inocula of extended-spectrum beta-lactamase and non-ESBL producing Klebsiella pneumoniae, *Diagn. Microbiol. Infect. Dis.* **49**, 41–46 (2004).

180. K. I. Udekwu, N. Parrish, P. Ankomah, F. Baquero, B. R. Levin, Functional relationship between bacterial cell density and the efficacy of antibiotics, *J. Antimicrob. Chemother.* **63**, 745–757 (2009).

181. M. R. Jacobs, Optimisation of antimicrobial therapy using pharmacokinetic and pharmacodynamic parameters, *Clin. Microbiol. Infect.* **7**, 589–596 (2001).

182. M. E. Falagas, G. S. Tansarli, P. I. Rafailidis, A. Kapaskelis, K. Z. Vardakas, Impact of antibiotic MIC on infection outcome in patients with susceptible gram-negative bacteria: A systematic review and meta-analysis, *Antimicrob. Agents Chemother.* **56**, 4214–4222 (2012).

183. U.S. Department of Health and Human Services Food and Drug Administration Center for Devices Radiological Health, *Class II Special Controls Guidance Document : Antimicrobial Susceptibility Test (AST) Systems* (Washington, DC, 2009).

184. B. Li, Y. Qiu, H. Shi, H. Yin, The importance of lag time extension in determining bacterial resistance to antibiotics, *Analyst* **141**, 3059–3067 (2016).

185. O. Fridman, A. Goldberg, I. Ronin, N. Shoresh, N. Q. Balaban, Optimization of lag time underlies antibiotic tolerance in evolved bacterial populations, *Nature* **513**, 418–421 (2014).

186. B. G. Spratt, Distinct penicillin binding proteins involved in the division, elongation, and shape of Escherichia coli K12, *Proc. Natl. Acad. Sci.* **72**, 2999–3003 (1975).

187. T. S. J. Elliott, A. Shelton, D. Greenwood, The response of Escherichia coli to ciprofloxacin and norfloxacin, *J. Med. Microbiol.* **23**, 83–88 (1987).

188. D. J. Mason, E. G. M. Power, H. Talsania, I. Phillips, V. A. Gant, Antibacterial action of ciprofloxacin, *Antimicrob. Agents Chemother.* **39**, 2752–2758 (1995).

189. K. Chen, G. W. Sun, K. L. Chua, Y. H. Gan, Modified virulence of antibiotic-induced Burkholderia pseudomallei filaments, *Antimicrob. Agents Chemother.* **49**, 1002–1009 (2005).

190. C. J. Ingham, M. Van Den Ende, P. C. Wever, P. M. Schneeberger, Rapid antibiotic sensitivity testing and trimethoprim-mediated filamentation of clinical isolates of the Enterobacteriaceae assayed on a novel porous culture support, *J. Med. Microbiol.* **55**, 1511–1519 (2006).

191. D. O. Serra, A. M. Richter, R. Hengge, Cellulose as an architectural element in spatially structured Escherichia coli biofilms, *J. Bacteriol.* **195**, 5540–5554 (2013).

192. N. J. Holden, Switches, cross-talk and memory in Escherichia coli adherence, *J. Med. Microbiol.* **53**, 585–593 (2004).

193. R. R. Spurbeck, A. E. Stapleton, J. R. Johnson, S. T. Walk, T. M. Hooton, H. L. T. Mobley, Fimbrial profiles predict virulence of uropathogenic Escherichia coli strains: contribution of ygi and yad fimbriae, *Infect. Immun.* **79**, 4753–63 (2011).

194. B. K. Dhakal, M. A. Mulvey, The UPEC pore-forming toxin α-hemolysin triggers proteolysis of host proteins to disrupt cell adhesion, inflammatory, and survival pathways, *Cell Host Microbe* **11**, 58–69 (2012).

195. K. M. Bennett, S. L. Walker, D. D. Lo, Epithelial microvilli establish an electrostatic barrier to microbial adhesion, *Infect. Immun.* **82**, 2860–2871 (2014).

196. K. Melican, J. Boekel, L. E. Månsson, R. M. Sandoval, G. A. Tanner, O. Källskog, F. Palm, B. A. Molitoris, A. Richter-Dahlfors, Bacterial infection-mediated mucosal signalling induces local renal ischaemia as a defence against sepsis, *Cell. Microbiol.* **10**, 1987–1998 (2008).

197. H. Kimura, Y. Sakai, T. Fujii, Organ/body-on-a-chip based on microfluidic technology for drug discovery, *Drug Metab. Pharmacokinet.* **33**, 43–48 (2018).

198. J. Boekel, Ö. Källskog, M. Rydén-Aulin, M. Rhen, A. Richter-Dahlfors, Comparative tissue transcriptomics reveal prompt inter-organ communication in response to local bacterial kidney infection, *BMC Genomics* **12**, 123 (2011).

199. W. M. S. Russell, R. L. Burch, *The principles of humane experimental technique* (Methuen, London, 1959).

200. D. M. Updegraff, Semimicro determination of cellulose in biological materials, *Anal. Biochem.* **32**, 420–424 (1969).

201. J. B. Sluiter, R. O. Ruiz, C. J. Scarlata, A. D. Sluiter, D. W. Templeton, Compositional analysis of lignocellulosic feedstocks. 1. Review and description of methods, *J. Agric. Food Chem.* **58**, 9043–9053 (2010).